Title
Dissecting the contribution of host genetics and the microbiome in complex behaviors

Journal
Cell, 184(7)

ISSN
0092-8674

Authors
Buffington, Shelly A
Dooling, Sean W
Sgritta, Martina
et al.

Publication Date
2021-04-01

DOI
10.1016/j.cell.2021.02.009

Peer reviewed

HHS Public Access

Author manuscript

Cell. Author manuscript; available in PMC 2022 April 11.

Published in final edited form as:

Cell. 2021 April 01; 184(7): 1740–1756.e16. doi:10.1016/j.cell.2021.02.009.

Dissecting the contribution of host genetics and the microbiome in complex behaviors

Shelly A. Buffington[1,2,6,†], **Sean W. Dooling**[1,2,3,†], **Martina Sgritta**[1,2], **Cecilia Noecker**[4], **Oscar D. Murillo**[3], **Daniela F. Felice**[1,2], **Peter J. Turnbaugh**[4,5], **Mauro Costa-Mattioli**[1,2,3,7,*]

[1]Department of Neuroscience, Baylor College of Medicine, Houston, TX 77030, USA.

[2]Memory and Brain Research Center, Baylor College of Medicine, Houston, TX 77030, USA.

[3]Department of Molecular & Human Genetics, Baylor College of Medicine, Houston, TX 77030, USA.

[4]Department of Microbiology & Immunology, University of California, San Francisco, CA, 94143, USA.

[5]Chan Zuckerberg Biohub, San Francisco, CA 94158, USA

[6]Current address: Department of Neuroscience, Cell Biology, & Anatomy, University of Texas Medical Branch, Galveston, TX 77555, USA.

[7]Lead contact,

SUMMARY

The core symptoms of many neurological disorders have traditionally been thought to be caused by genetic variants affecting brain development and function. However, the gut microbiome, another important source of variation, can also influence specific behaviors. Thus, it is critical to unravel the contributions of host genetic variation, the microbiome, and their interactions to complex behaviors. Unexpectedly, we discovered that different maladaptive behaviors are interdependently regulated by the microbiome and host genes in the *Cntnap2*$^{-/-}$ model for neurodevelopmental disorders. The hyperactivity phenotype of *Cntnap2*$^{-/-}$ mice is caused by host genetics, whereas the social behavior phenotype is mediated by the gut microbiome. Interestingly, specific microbial intervention selectively rescued the social deficits in *Cntnap2*$^{-/-}$ mice through upregulation of metabolites in the tetrahydrobiopterin synthesis pathway. Our findings that behavioral abnormalities could have distinct origins (host genetic vs microbial) may change the way we think about neurological disorders and how to treat them.

*Correspondence to: Mauro Costa-Mattioli (costamat@bcm.edu).

†These authors contributed equally to this work.

Author contributions: Conceptualization and design, S.A.B., S.W.D., M.C.-M.; Acquisition & Analysis of Data, S.A.B., S.W.D., M.S., C.N., O.D.M., D.F.F., P.J.T.; Writing, Reviewing, & Editing, S.A.B., S.W.D., M.S., C.N., P.J.T., M.C.-M.

Declaration of interest: A patent application related to the role of *L. reuteri* on social behavior has been filed by BCM. Findings regarding the manipulation of endogenous biotperin levels by the microbiome are the subject of a provisional patent application owned by BCM. M.C.-M. is a scientific co-founder of Mirkrovia. The authors declare no other conflicts of interest.

In brief:

Host genetics and the microbiome interdependently regulate maladaptive behaviors in a mouse model for neurodevelopmental disorders. Precise microbial, or microbe-induced metabolite-based therapy, selectively rescues social deficits but not hyperactivity.

Graphical Abstarct

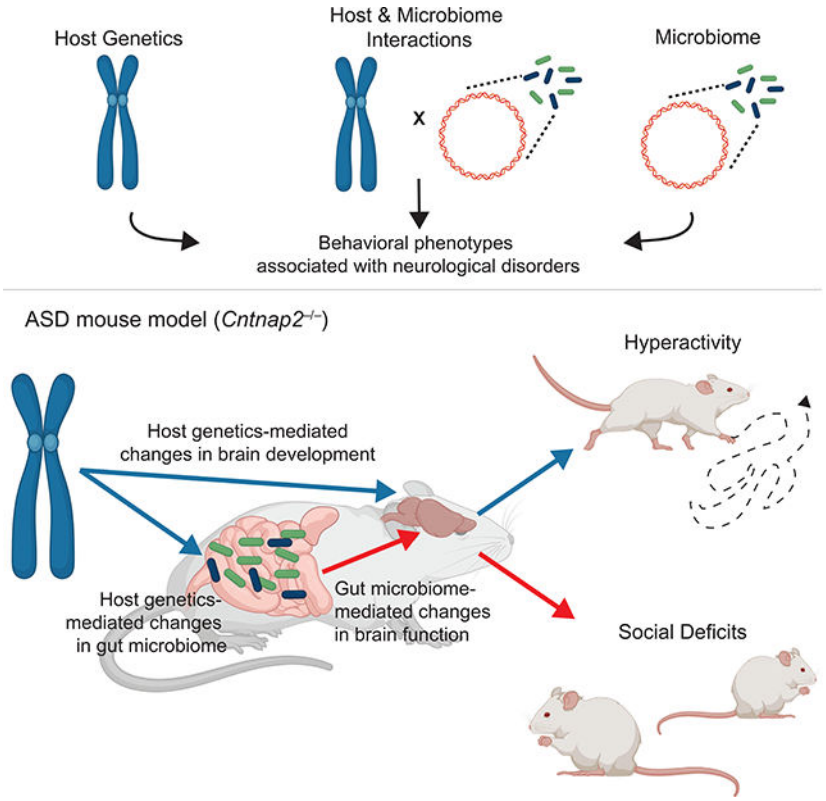

Keywords

oxytocin; hologenome; neurological disorders; social behavior; hyperactivity; *L. reuteri* ; tetrahydrobiopterin; gut-brain-axis

INTRODUCTION

It is traditionally believed that by directly impacting brain development and function, genetic variants are the primary drivers of the behavioral symptoms associated with neurological disorders (Sahin and Sur, 2015; Silva and Ehninger, 2009). Indeed, most of the current research in neurogenetics focuses on how genetic variants associated with neurological disorders i) regulate activity in key brain regions in human (e.g., using sophisticated imaging techniques), ii) hijack the function of relevant molecular pathways (e.g., using molecular and cell-specific genetic approaches), and/or iii) modulate selective circuits in the brain (e.g., using opto- and chemo-genetics) that give rise to overt behavioral and internal neuronal

states. Consequently, current therapeutic approaches for neurological disorders aim to target the brain directly.

In addition to host genetics, which can explain certain phenotypic changes, the microbiome is another important source of variation (Fischbach and Segre, 2016). Indeed, we, individuals, are the bearers not only of our own cells and genes, but also of the microorganisms (and their genes) living with us. Thus, the phenotypes of an individual may arise from complex interactions between the genetics of the host and microorganisms, which led to the notion of the holobiont [an animal or plant host together with all associated microorganisms living in symbiosis with it (Margulis, 1993)] and the hologenome [(Rosenberg et al., 2007), the sum of all microbial genes plus the genes of the host].

Given that genetic variation is able to influence the gut microbial ecology (Benson et al., 2010; Elinav et al., 2011; Goodrich et al., 2014; Khachatryan et al., 2008; Rehman et al., 2011) and that the gut microbiota can modulate host behaviors associated with neurological dysfunction in a very powerful manner *via* the gut-brain axis [reviewed in (Sharon et al., 2016; Sherwin et al., 2019; Vuong et al., 2017)], it is essential to dissect whether different complex behaviors in genetic neurological disorders could result from reciprocal host-microbiota interactions. Investigating the mechanisms through which host and microbial factors regulate complex behaviors will not only expand our understanding of neurological disorders but may also lead to new therapies.

RESULTS

Different breeding schemes modulate behavior and microbiota composition in a genetic mouse model for neurodevelopmental disorders.

To study the role of host-microbiome interactions in complex behaviors, we employed the *Cntnap2*$^{-/-}$ mouse model for neurodevelopmental disorders. Consistent with some of the behavioral abnormalities observed in individuals with mutations in *CNTNAP2*, loss of *Cntnap2* [contactin-associated protein-like 2; which encodes the protein Caspr2 (Poliak et al., 1999; Poliak et al., 2001)], in mice leads to social deficits and hyperactivity (Bakkaloglu et al., 2008; O'Roak et al., 2011; Peñagarikano et al., 2011; Peñagarikano et al., 2015).

We first tested social behavior in wild-type (WT; *Cntnap2*$^{+/+}$) and knockout (KO; *Cntnap2*$^{-/-}$) mice born from isolated homozygous breeding lines (Isolated lines: WT-I and KO-I, respectively; Fig. 1A,B and S1A) using the 3-chamber test for sociability and social novelty. As expected, we found that WT-I mice spent significantly more time interacting with the stranger mouse (Mouse 1) than with the empty cup (Empty), indicating normal sociability (Fig. 1C). By contrast, KO-I mice exhibited impaired sociability as evidenced by their lack of social preference (Fig. 1C), as previously reported (Peñagarikano et al., 2011; Peñagarikano et al., 2015). Moreover, unlike WT-I, KO-I mice did not prefer to interact with a novel mouse (Mouse 2) over a familiar mouse (Mouse 1) in the social novelty test (Fig. 1D). Accordingly, in a reciprocal social interaction test, KO-I mice spent less time interacting with each other compared to WT-I mice (Fig. 1E). KO-I mice displayed no deficits in olfaction compared to WT-I mice as measured in the buried food test (Mann-Whitney $U = 66$, $P = 0.7444$), indicating that their social deficits were not likely due to

impaired olfaction. Moreover, when we assessed their locomotor activity in the 3-chamber test, we found that KO-I mice were hyperactive compared to WT-I mice (Fig. 1F,G), consistent with previous reports (Peñagarikano et al., 2011; Peñagarikano et al., 2015). Thus, *Cntnap2*$^{-/-}$ mice generated from isolated breeding (KO-I) show impaired social behavior and hyperactivity.

Individuals with neurodevelopmental disorders, such as autism spectrum disorders (ASD), often present with gastrointestinal comorbidities and an altered microbiome composition (De Angelis et al., 2013; Finegold et al., 2010; Strati et al., 2017; Vuong and Hsiao, 2017). Thus, we next examined whether KO-I mice show alterations in their gut microbial ecology using 16S ribosomal RNA (rRNA) gene sequencing. Analysis of beta (between subject) diversity revealed that KO-I mice harbor an intestinal microbial composition distinct from WT-I mice. To measure beta diversity, we used three independent metrics: principal components analysis (PCA) with PhILR (Phylogenetic Isometric Log-Ratio)-transformed Euclidean distances (Silverman et al., 2017) (Fig. 1H) and principal coordinates analysis (PCoA) with Bray-Curtis (Fig. S1B) or unweighted UniFrac dissimilarities (Fig S1C). Analysis of alpha (within subject) diversity quantified by the Shannon diversity index and richness showed that KO-I mice have increased diversity compared to WT-I mice (Fig. S1D,E). Additionally, 33 amplicon sequence variants (ASVs) were differentially abundant in KO-I mice compared to WT-I mice (Fig. 1I, S1F, Table S1) as well as 33 predicted microbial metabolic pathways inferred by PICRUSt2 (Fig. S1G,H, Table S2). Thus, *Cntnap2*$^{-/-}$ mice originating from the isolated line (KO-I) show differences in their gut microbiota.

Conclusive evidence that a genomic mutation is responsible for a specific phenotype, such as impaired behavior, can only be obtained when littermate controls are used (Holmdahl and Malissen, 2012; Stappenbeck and Virgin, 2016). Thus, we performed experiments using *Cntnap2*$^{-/-}$ mice and *Cntnap2*$^{+/+}$ littermate controls, which were born from a heterozygous breeding line (Littermate line: KO-L and WT-L, respectively; Fig. 2A,B and Fig. S1I). Surprisingly, unlike KO-I mice, KO-L mice showed normal social behavior (Fig. 2C–E). In contrast, like KO-I mice, KO-L mice were hyperactive compared to WT-L mice (Fig. 2F,G). In accordance with the social behavior results, KO-L and WT-L mice exhibited a similar composition of their gut microbiota with no changes in alpha or beta diversity (Fig. 2H, S1J–M), abundance of ASVs (Fig. 2I, S1N, Table S1), or predicted microbial metabolic pathways (Fig. S1O,P, Table S2). Thus, *Cntnap2*$^{-/-}$ mice originated from the littermate line (KO-L) exhibit hyperactivity, but normal social behavior and similar gut microbiota to wild-type littermates (WT-L).

The microbiome selectively modulates social behavior, but not locomotor activity levels, in a genetic mouse model for neurodevelopmental disorders.

Littermate controls are considered to be the gold-standard in behavioral neuroscience since they help to establish the contribution of host genes over environmental factors onto a given phenotype. However, if the microbiome directly modulates a given behavior, the phenotype of the mutant animal may be masked by co-housing conditions. For example, we know now that behavioral deficits can emerge as a result of the lack of one or more bacterial species [reviwed in (Hsiao et al., 2013; Lynch and Hsiao, 2019; Olson et al., 2018; Sherwin et al.,

2019)]. If WT and mutant mice are littermates and consequently co-housed in the same cage, a bacterial species that confers a given phenotype and is missing in the mutant mice can be transferred from the WT to the mutant mice (Ridaura et al., 2013). Given that the social deficits and changes in microbiota composition observed in KO-I mice are absent in KO-L mice that were housed with WT-L littermates, but the hyperactivity phenotype is observed in both mutant lines (KO-I and KO-L), we hypothesized that the social phenotype is driven by the gut microbiome, whereas the locomotor activity phenotype is only mediated by the *Cntnap2* mutation in the host.

To test this hypothesis and isolate the potential effect of host versus microbial genetics on behavior, we i) co-housed *Cntnap2*$^{-/-}$ mice originated from the isolated line (KO-I) with WT mice (WT-I), ii) separated *Cntnap2*$^{-/-}$ mice originated from the littermate line (KO-L) from WT-L mice and iii) performed fecal microbiota transplant (FMT) of both littermate and isolated lines into germ-free (GF) mice that are reared in the total absence of microorganisms.

First, co-housing KO-I with WT-I mice (Fig. 3A,B and Fig. S2A), which allows the passive interchange of gut microbiota between hosts, led to a more similar microbiota composition. Briefly, there were no significant differences in ASVs or predicted metabolic pathways (Fig. 3I, S2F–H, Table S1, S2) between co-housed WT-I and KO-I mice. Accordingly, alpha diversity assessed by the Shannon diversity index (Fig. S2D) and beta diversity assessed by PCoA with Bray-Curtis and unweighted UniFrac dissimilarities were similar in co-housed KO-I and WT-I (Fig. S2B,C). However, alpha diversity determined by richness (Fig. S2E) and beta diversity determined by PCA of PhILR-transformed Euclidean distances (Fig. 3H) showed a modest difference between the two groups (PERMANOVA $R^2 = 0.11$, P-value = 0.044) compared to the difference observed in the isolated lines (WT-I and KO-I mice, see Fig 1H, PERMANOVA $R^2 = 0.36$, $P = 0.0002$). Hence, co-housing led to a more similar composition of the gut microbiota between groups.

Importantly, co-housed KO-I mice no longer displayed deficits in social behaviors (Fig. 3C–E), but remained hyperactive (Fig. 3F,G). Thus, co-housing rescues the social deficits, but not hyperactivity phenotype, in *Cntnap2*$^{-/-}$ mice originated from the isolated line (KO-I).

Second, likely due to the inherent nature of their breeding scheme, WT-L mice and KO-L mice cohabitate and carry a similar microbiota composition (Fig. 2H,I, Fig S1I–N). We next wondered whether separation of WT-L and KO-L mice would lead to a shift in their microbiome profile and ultimately deficits in social behavior. To answer this question, WT-L and KO-L mice were separated according to their genotype at weaning and bred as adults to generate transgenerational WT and KO mice (WT-T and KO-T) (Fig. 4A,B and Fig. S2I). While KO-T mice still showed normal sociability (Fig 4C), social novelty was impaired in these mice (Fig. 4D). It is noteworthy that the social novelty test in rodents is used to evaluate components of social affiliation and social recognition and deficits in these behaviors are described as central in ASD (American Psychiatric Association, 2013). Moreover, normal sociability and impaired social novelty has been observed in several mouse models for ASD (Carter et al., 2011; Chen et al., 2019; Jiang and Ehlers, 2013; Kazdoba et al., 2016; Liu and Smith, 2009; Pietropaolo et al., 2011). In addition to the

deficits in social novelty, KO-T mice also exhibit deficits in reciprocal social interaction (Fig. 4E). Thus, given that KO-T mice are deficient in two out of the three social tasks, we conclude that they show deficits in social behavior. Additionally, the KO-T mice were hyperactive compared to WT-T controls (Fig. 4F,G).

Consistent with the hypothesis that social behavior (but not locomotor activity levels) is regulated by the gut microbiome, we found that KO-T mice exhibit a different gut microbiota composition (Fig. 4H,I, S2J–N). We also identified significant changes in the abundance of 73 ASVs (Fig 4I, S2N, Table S1) and 44 predicted microbial metabolic pathways in KO-T mice compared to WT-T mice (Fig. S2O,P, Table S2). Thus, separation experiments negatively altered social behaviors and led to changes in the microbiota composition in KO-T mice, but did not change the hyperactivity phenotype observed in *Cntnap2*$^{-/-}$ mice originated from the littermate line (KO-L).

Finally, to rule out a potential influence of maternal care and other variables on behavior and to causally test whether changes in the microbiome modulate social behavior in *Cntnap2*$^{-/-}$ mice, we performed FMTs from donors of the isolated (WT-I and KO-I) and littermate (WT-L and KO-L) lines into GF mice (Fig. 5A). After transplantation into GF mice, the microbial communities from the different groups largely maintained their identity (Fig. S3, Table S1, S2) as seen in other FMT models (Ang et al., 2020). In behavioral analyses, GF mice showed impaired sociability and preference for social novelty (Fig. 5B,C), consistent with previous reports (Buffington et al., 2016; Desbonnet et al., 2014; Sgritta et al., 2019). More importantly, we found that the behavior of the GF recipient mice mirrored that of their respective microbiota donors. Specifically, FMT with WT-sourced microbiota (i.e., GF:WT-I, GF:WT-L) rescued social deficits in GF mice regardless of the donor line (Fig. 5B,C). However, the social deficits in GF mice were only reversed by FMT with KO-L-sourced microbiota (i.e., GF:KO-L), but not by KO-I-sourced microbiota (i.e., GF:KO-I; Fig. 5B,C). Thus, these data indicate that *Cntnap2*$^{-/-}$ mice originated from the isolated line (KO-I) may lack one or more bacterial species that are crucially required for social behavior. Given that FMT does not lead to changes in hyperactivity in any of the GF mice (Fig. 5D,E), our results provide causal evidence that the social deficits in *Cntnap2*$^{-/-}$ mice are mediated by alterations in the microbiome.

Selective microbial intervention rescues social deficits, but not hyperactivity, in a genetic mouse model for neurodevelopmental disorders.

While we provide a characterization of the microbiome of *Cntnap2*$^{-/-}$ mice, previous studies have focused on specific brain circuits. In particular, the oxytocinergic system, which is known to modulate numerous aspects of social behaviors and is implicated in ASD (Donaldson and Young, 2008; LoParo and Waldman, 2015), has been reported to be deficient in *Cntnap2*$^{-/-}$ mice (Peñagarikano et al., 2015). In *Cntnap2*$^{-/-}$ mice, the paraventricular nuclei (PVN) of the hypothalamus, where oxytocin is primarily synthesized, contain less oxytocin producing neurons and oxytocin treatment reverses the social deficits in the mutant mice (Peñagarikano et al., 2015). Accordingly, we found that intranasal oxytocin treatment reversed the social deficits, but not the hyperactivity, in *Cntnap2*$^{-/-}$ (KO-I) mice (Fig. S4A–F).

We and others have previously shown that microbial intervention with the commensal bacterial species *Lactobacillus reuteri* promotes oxytocin levels in plasma and the PVN (Buffington et al., 2016; Poutahidis et al., 2013; Sgritta et al., 2019) and reverses social deficits in several mouse models for ASD (Buffington et al., 2016; Sgritta et al., 2019; Tabouy et al., 2018). However, the same manipulation failed to do so in mice with deficient oxytocin receptors (Sgritta et al., 2019). Thus, we next wondered whether *L. reuteri* treatment could rescue the social behavior deficits in the *Cntanp2*$^{-/-}$ mice. First, we examined whether *L. reuteri* levels are altered in *Cntnap2*$^{-/-}$ (KO-I) mice and found that *L. reuteri* levels were reduced in KO-I mice as determined by qPCR (Fig. S5A). Second, we found that treatment with *L. reuteri* reversed the deficits in oxytocin producing neurons in KO-I mice (Fig. S4G–J). Third, and more notably, we found that *L. reuteri* treatment reversed the social deficits in both young (Fig. 6A–C,G) and adult KO-I mice (Fig. S5B–D). Fourth, the same microbial intervention did not affect the hyperactivity phenotype in KO-I mice (Fig. 6D,E). Thus, early or late precision microbial intervention selectively reverses the social deficits, but not the hyperactivity phenotype, in *Cntnap2*$^{-/-}$ (KO-I) mice, supporting the notion that social and locomotor activity phenotypes have different hologenomic origins.

Selective microbial intervention rescues social interaction-induced synaptic transmission in the ventral tegmental area (VTA) of a genetic mouse model for neurodevelopmental disorders.

Brain regions responding to naturally rewarding stimuli, including the VTA, are crucially involved in social behavior. More specifically, oxytocin-expressing neurons in the PVN project to dopaminergic (DA) neurons of the VTA (Melis et al., 2007) and the activation of DA neurons by oxytocin within this circuit is critically required for social behavior (Gunaydin et al., 2014; Hung et al., 2017; Xiao et al., 2017). Consistent with the idea that social stimulation can be particularly rewarding, we and others found that social interaction triggers synaptic strengthening in VTA DA neurons of birds (Huang and Hessler, 2008) and mice (Bariselli et al., 2018; Buffington et al., 2016; Sgritta et al., 2019), as determined by measuring the ratio of alpha-amino-3-hydroxy-5-methyl-4-isoxazolepropionic acid receptor (AMPAR) to N-methyl-d-aspartate receptor (NMDAR) currents. Interestingly, this potential cellular correlate of social interaction, namely social interaction-evoked synaptic transmission in VTA DA neurons, is impaired in ASD models exhibiting social deficits (Buffington et al., 2016; Sgritta et al., 2019). In addition, *L. reuteri* treatment reverses the synaptic deficits in different ASD mouse models in an oxytocin-dependent manner (Buffington et al., 2016; Sgritta et al., 2019). We found that social interaction failed to induce an increase in the AMPAR/NMDAR ratio in KO-I VTA neurons compared to those of control mice (Fig. 6F,H). Conversely, cocaine administration induced an increase in the AMPAR/NMDAR ratio in VTA DA neurons, indicating that DA neurons were functional and responsive to a rewarding, but not a social reward stimulus (Fig. 6H). More importantly, treatment with *L. reuteri* rescued the deficits in social interaction-induced synaptic plasticity in VTA DA neurons from *Cntnap2*$^{-/-}$ (KO-I) mice (Fig. 6H), reinforcing the notion that *L. reuteri* enhances the salience and rewarding value of social stimuli.

To assess whether *L. reuteri* affects synaptic transmission in other brain regions implicated in social behavior (Huang et al., 2020), we measured miniature excitatory post synaptic

currents (mEPSCs) in the medial prefrontal cortex (mPFC) of *Cntnap2*$^{-/-}$ (KO-I) and WT-I mice. Consistent with previous results (Lazaro et al., 2019), the amplitude and frequency of mEPSCs in pyramidal neurons from mPFC were reduced in KO-I mice compared to WT-I mice (Fig. 6I–K). Treatment with *L. reuteri* failed to reverse the changes in mEPSCs in KO-I mice (Fig. 6I–K). These data indicate that *L. reuteri* modulates changes in synaptic transmission selectively in the VTA, but not in the mPFC.

Taken together, selective microbial intervention with *L. reuteri* rescues the social behavior and social behavior related-plasticity deficits, but not the hyperactivity phenotype, in *Cntnap2*$^{-/-}$ (KO-I) mice.

Microbially-induced restoration of select metabolites reverses social and synaptic deficits, but not hyperactivity, in a genetic mouse model for neurodevelopmental disorders.

Metabolites produced or induced by gut microorganisms could signal beyond the gastrointestinal tract and modulate brain functions *via* the gut microbiota-to-brain signaling systems (Mayer et al., 2015; Sherwin et al., 2019). To investigate the mechanism by which *L. reuteri* reverses the social deficits in KO-I mice, we performed unbiased gut metabolomic profiling. Unsupervised hierarchical clustering analysis revealed that the metabolomic profile of KO-I mice is markedly different from that of WT-I mice (Fig. 7A) and that treatment with *L. reuteri* did not shift the overall metabolomic profile of the KO-I mice back to a WT-I state (Fig. 7A). Given this, we next wondered whether there were changes in selective metabolites that could help to differentiate the socially normal (WT-I, KO-I + *L. reuteri*) from the socially deficient mice (KO-I). Random forest analysis revealed that the top two most discriminatory metabolites between the socially normal and deficient mice were biopterin and dihydrobiopterin (BH2), two metabolites in the tetrahydrobiopterin (BH4) metabolism pathway (Fig. 7B). More importantly, the level of these metabolites was significantly reduced in KO-I mice compared with WT-I and was fully rescued by treatment with *L. reuteri* (Fig. 7C,D).

BH4 is the biologically active biopterin molecule that serves as co-factor for a number of important enzymes that produce neuroactive molecules such as dopamine, serotonin, and nitric oxide (Thony et al., 2000). Because *L. reuteri* promotes the level of metabolites in the BH4 pathway (Fig. 7C,D) and reverses the social deficits but not the hyperactivity phenotype in KO-I mice (Fig. 6B–E, G), and because the social deficits in KO-I mice are mediated by the microbiome (Fig. 1–5, Fig. S1–S3), we wondered whether BH4 treatment alone would be sufficient to selectively reverse the social deficits in KO-I mice. To answer this question, KO-I mice were treated with BH4 (or vehicle) *via* oral gavage (Fig. 7E). Remarkably, like treatment with *L. reuteri*, treatment with BH4 alone reversed the social deficits (Fig. 7F,G,I) and the impaired social reward-related synaptic plasticity in VTA DA neurons (Fig. 7H,J). In contrast, treatment with BH4 failed to reverse the hyperactivity phenotype in KO-I mice (Fig. 7K,L), further strengthening the notion that the social deficits are mediated by changes in the microbiome and the hyperactivity phenotype is modulated by host genes. Thus, *L. reuteri* reverses social and synaptic plasticity deficits, at least, in part, by modulating the host's endogenous levels of tetrahydrobiopterin in the gut.

To examine whether BH4 exerts its effect on social behavior directly or through changing the microbiome, we next examined whether BH4 could rescue the social deficits in GF mice (Fig. S6A). Consistent with our previous findings that mono-colonization of GF mice with *L. reuteri* rescued their social deficits (Sgritta et al., 2019), we found that BH4 also reversed the social deficits in GF mice (Fig. S6B,C). As expected, BH4 had no effect on the activity levels of GF mice (Fig. S6D,E). These findings provide another line of evidence that the social behavior phenotype of *Cntnap2*$^{-/-}$ mice is mediated by the gut microbiome, whereas the hyperactivity phenotype is caused by host genetics.

Having shown that BH4 is sufficient for social behavior, we next asked whether the effect of *L. reuteri* on social behavior depends on the biopterin pathway. To answer this question, *Cntnap2*$^{-/-}$ (KO-I) mice treated with *L. reuteri* were injected with SPRi3 (Fig. S7A), a potent and selective inhibitor of sepiapterin reductase, the final enzyme in the BH4 synthesis pathway (Cronin et al., 2018; Latremoliere et al., 2015). Interestingly, when BH4 synthesis was pharmacologically blocked, *L. reuteri* failed to rescue the social deficits in KO-I mice (Fig. S7B–D), indicating that *L. reuteri* rescues the social deficits through modulating the host's BH4 system. It is noteworthy that SPRi3 did not affect the locomotor activity of *L. reuteri*-treated KO-I mice (Fig. S7E,F), reinforcing the idea that social deficits and hyperactivity have a different origin.

Finally, we examined whether BH4 is necessary for normal social behavior in WT mice (Fig. S7G). We found that pharmacological inhibition of BH4 synthesis with SPRi3 impaired social behavior in WT mice (Fig. S7H–J), but did not significantly alter locomotor activity (Fig. S7K,L). Thus, the BH4 system is selectively required for normal social behavior.

DISCUSSION

We now know that many aspects of an individual's physiology and behavior can be greatly influenced by variation in both the host's genome and microbiome [reviewed in (Lynch and Hsiao, 2019; Sharon et al., 2016; Sherwin et al., 2019; Vuong et al., 2017)]. Until now, the contribution of host genes and microbial genes on a mouse behavioral phenotype have been considered separately. Given that we are composite of not only our own genes but also microorganisms and their interactions (Fischbach and Segre, 2016), it is crucial to understand whether the symptoms in a given neurological disorder are caused by the direct impact of host genetic variation on brain function or by alterations of the host's gut-microbiome-brain axis. Strikingly, we found that distinct maladaptive behaviors have different hologenomic etiologies. More specifically, using 7 independent approaches (co-housing, separation experiments, microbiota transplantation into GF mice, selective *L. reuteri* reconstitution, selective BH4-treatment, oxytocin-treatment, and SPRi3-treatment) as well as genetic and amplicon sequencing analyses, here we provide convergent evidence that, in a genetic mouse model for neurodevelopmental disorders, the social behavior phenotype is determined by gut microbiome whereas the animal's locomotor activity levels are directly modulated by the host genetic allele.

We also found that treatment with *L. reuteri* at different developmental stages is able to selectively rescue the social deficits in *Cntnap2*$^{-/-}$ mice, indicating a wide temporal window for microbial-based restoration of social behavior. Moreover, using unbiased metabolomics analyses, we provide evidence that *L. reuteri* boosts the host's endogenous BH4 synthesis pathway and that direct administration of BH4 to the animal's gut, independent of any microbial intervention, also rescues social behavior and related changes in synaptic function without affecting activity levels. In subsequent experiments, it will be interesting to identify other bacterial species that either produce or induce BH4 and examine whether they are able to promote social behavior.

Previously, we have shown that *L. reuteri* signals to the brain and modulates social behavior *via* the vagus nerve and the oxytocinergic system (Sgritta et al., 2019). More specifically, either surgical cutting of the vagus nerve or inhibition of oxytocin receptors in DA neurons prevents the prosocial effect mediated by *L. reuteri* (Sgritta et al., 2019). Interestingly, BH4 has been shown to increase oxytocin release in rats (Ciosek and Guzek, 1992; Ciosek et al., 1992) and we found that BH4 failed to reverse social deficits in KO-I mice that were treated with a selective and potent oxytocin receptor antagonist compared to vehicle treated KO-I mice (Fig. S6F,G). Future experiments will examine the specific action of BH4 and whether its effect is mediated by the vagus nerve. Finally, the BH4 findings are particularly interesting since studies in humans have shown that BH4 treatment improves some clinical symptoms, including social behavior-related symptoms, in individuals with ASD (Klaiman et al., 2013).

Moreover, our findings also indicate that it is extremely important to consider the role of the microbiome in behavioral neuroscience. Undoubtedly, to control for genomic and microbial variations the use of littermate controls should be the gold standard. However, if microbiota are a contributing factor, some of the phenotypes can be masked due to co-housing conditions, as we showed here for the social behavior in *Cntnap2*$^{-/-}$ mice. Indeed, these findings raise the interesting possibility that phenotypes seen in other genetic models of disease (e.g., diabetes, cancer, immunity, viral infection, neurological disorders) can be mediated by host genetics, changes in the microbiome, and/or their interactions. Thus, in future experiments, it will be essential to embrace the complexity of the hologenome in order to fully understand the etiology of different behaviors. Taking into account previously unconsidered variables, such as gut microbiota composition, breeding schemes, and host-microbiome interactions, should enhance not only the reproducibility of the findings (Stappenbeck and Virgin, 2016), but also the value of the research and its therapeutic potential across different animal models for neurological disorders.

Finally, given the current brain-centric view of genetic neurological disorders, we believe that our results widen our understanding of how a genetic mutation leads to behavioral abnormalities. In addition, they suggest that both brain and gut-microbiota may need to be targeted to fully and effectively reverse the core symptoms associated with some neurological disorders.

LIMITATIONS AND FUTURE DIRECTIONS

Here we show that a given symptom (or behavioral abnormality) in a genetic brain disorder could arise through the combined interactions of host genetics and microbiome. Additional work will be necessary to fully understand the mechanisms underlying this phenomenon. These include a) the study of how the loss of *Cntnap2* results in alterations in gut microbiota composition and b) the precise mechanism by which BH4 is produced and signals to the brain. It will be also interstesting to determine whether our findings are generalizable and extend to other complex behaviors and/or diseases. For instance, do other genetic variants modulate behavior and brain function via host genetics and microbiome interactions? Are other diseases, such as obesity, cancer, metabolic disorders, and immunity also subject to host genetic-microbiome control? If so, can we leverage this knowlwege to develop precision medicine for specific genetic disorders based on new microbial-based therapies?

STAR Methods

RESOURCE AVAILABILITY

Lead Contact—Further information and reasonable requests for resources and reagents should be directed to and will be fulfilled by the Lead Contact, Mauro Costa-Mattioli (costamat@bcm.edu).

Materials Availability—This study did not generate new unique reagents. Information on reagents used in this study is available in the Key Resources Table.

Data and Code Availability—The the sequencing data reported in this paper is available through NCBI Sequence Read Archive: BioProject PRJNA683064. All other data needed to evaluate the conclusions in the paper are present in the paper and/or supplementary materials.

EXPERIMENTAL MODEL AND SUBJECT DETAILS

Mouse Husbandry.—WT C57BL/6J (stock #000664) and *Cntnap2*$^{-/-}$ (*Cntnap2*^{tm1Pele}, stock # 017482) (Poliak et al., 2003) were obtained from Jackson Laboratories (Bar Harbor, ME). WT-I and KO-I mice were generated by breeding WT and *Cntnap2*$^{-/-}$ obtained from Jackson Laboratories. WT-L and KO-L mice were generated by breeding *Cntnap2*$^{+/-}$ mice derived by crossing *Cntnap2*$^{-/-}$ and WT (C57BL/6J) mice obtained from Jackson Laboratories. Germ-free (GF) mice (C57BL/6J) were housed in a flexible isolator fed with HEPA-filtered air and provided with irradiated food and water at the Baylor College of Medicine gnotobiotic facility. Subject mice were separated by sex at weaning and housed at 2–4 mice per cage. Consistent with previous studies using the *Cntnap2*$^{-/-}$ model (Peñagarikano et al., 2011; Peñagarikano et al., 2015), both male and female mice were used in this study. Experiments in this study were performed on 7–12 week-old mice. Animal care and experimental procedures were approved by Baylor College of Medicine's Institutional Animal Care and Use Committee in accordance with all guidelines set forth by the U.S. National Institutes of Health.

METHOD DETAILS

Fecal Microbiota Transplant.—Fresh fecal samples were collected from individual donor mice and homogenized on ice in sterile phosphate buffered saline (PBS) under sterile conditions. The resulting slurry was spun at 1,000g for 3 min at 4°C. The supernatants were isolated and diluted to 5×10^9 CFU/ml with sterile PBS. Four-week-old GF (C57BL/6J) recipient mice were then immediately colonized by a single gavage with 0.2 mL solution. Fecal samples were collected from the colonized GF mice at 1 day, 7 days, 14 days, 21 days, and 28 days following colonization. Fecal samples were snap frozen and stored at −80°C until prepared for sequencing. Behavioral experiments were initiated 4 weeks after the transplant.

Behavior Experiments.—All behavior experiments were conducted on mice aged 8–12 weeks unless otherwise stated. Mice were habituated to the experimenter for 3 days prior to the start of the behavioral experiment. All experiments were conducted during the light cycle.

3-Chamber Test.: Social behavior in the 3-Chamber Test was performed as previously described (Buffington et al., 2016; Sgritta et al., 2019; Silverman et al., 2010). Briefly, mice were first habituated for a 10-minute period in an empty 60 × 40 × 23 cm Plexiglas Arena divided into three equally-sized interconnected chambers (left, center, right). During habituation, the subject's position was continuously tracked using the automated tracking software, AnyMaze. Distance traveled and speed were automatically scored and used for measuring activity levels.

Sociability was evaluated during a second 10-minute period in which the subject could interact either with an empty wire cup (Empty) or a wire cup containing a stranger mouse (Mouse 1). Stranger mice were age- and sex-matched to the subject mouse. The interaction time was scored by measuring the time the subject mouse spent sniffing or climbing upon either the empty cup or the cup containing the stranger mouse. The position of the empty cup/stranger mouse in the left or right chamber during the sociability period was counterbalanced between trials, in order to avoid bias.

Preference for social novelty was evaluated, in a third 10-minute period, by introducing a second stranger mouse (Mouse 2) into the previously empty wire cup. The time spent interacting with either Mouse 1 or Mouse 2 was measured as mentioned above. Interaction time was scored using the automated AnyMaze software by trained, independent observers who were blind to the treatment group.

Reciprocal Social Interaction Test.: Reciprocal social interaction test was performed as previously described (Buffington et al., 2016; Sgritta et al., 2019). Mice were placed in a 25 × 25 × 25 cm Plexiglas neutral arena with a novel conspecific matched mouse according to genotype, age, sex, and/or treatment. Trained, independent observers recorded the time a pair of mice socially interacted, using the AnyMaze software. Interactions included close following, touching, nose-to-nose sniffing, nose-to-anus sniffing, grooming and/or crawling over/under each other. The human observers were blind to the treatment group.

16S rRNA Gene Sequencing.—16S rRNA gene sequencing was performed by the Center for Metagenomic & Microbiome Research at Baylor College of Medicine as previously described (Buffington et al., 2016; Sgritta et al., 2019). Methods were adapted from protocols developed for the NIH-Human Microbiome Project (Human Microbiome Project, 2012; Methé et al., 2012). Bacterial genomic DNA was extracted using MO BIO PowerSoil DNA Isolation Kit (MO BIO Laboratories). The 16S rDNA V4 region was amplified using PCR with primers 515F (5'-GTGCCAGCMGCCGCGGTAA-3') and 806R (5'-GGACTACHVGGGTWTCTAAT-3') (Caporaso et al., 2011) and sequenced on the MiSeq platform (Illumina) using the 2×250 bp paired-end protocol yielding paired-end reads that overlap almost completely. The primers used for amplification contained adapters for MiSeq sequencing and single-end barcodes allowing pooling and direct sequencing of PCR products.

The 16S rRNA gene read pairs were processed using QIIME2 v2020.6 (Bolyen et al., 2019). Reads were demultiplexed based on the unique molecular barcodes, trimmed to 220 base pairs in length for the forward reads and 140 base pairs for the reverse, denoised, merged, and filtered for chimeric reads with the DADA2 plugin (Callahan et al., 2016). 96.6% of the resulting amplicons were 252 or 253 base pairs in length, and amplicons less than 250 base pairs in length were discarded. Taxonomic assignments were generated for the resulting amplicon sequence variants (ASVs) by the taxonomic classifier in the DADA2 R package (version 1.10.0) using the SILVA database [version 138, (Quast et al., 2013)], with the option to add species-level information via exact matching where possible. For phylogenetic analyses, sequence variants were placed into the Greengenes 16S rRNA phylogeny using the SEPP QIIME2 plugin (Janssen et al., 2018). The median number of reads per sample before processing was 48,428 (minimum 9,445), and after processing, the median number of merged reads per sample was 32,224 (minimum 6,287).

Predictions of Microbial Gene Pathways.—Prediction of microbial gene pathways was performed using the Phylogenetic Investigation of Communities by Reconstruction of Unobserved States 2 (PICRUSt2) pipeline version 2.3.0-b (Douglas et al., 2020) with default parameters. In PICRUSt2, sequence variants are placed into a phylogenetic tree using EPA-NG (Barbera et al., 2019) and gappa (Czech et al., 2020), genomic hidden states are predicted using castor (Louca and Doebeli, 2018), and MetaCyc pathway abundances (Caspi et al., 2020) are inferred using MinPath (Ye and Doak, 2009).

Bacterial Quantification by quantitative PCR (qPCR).—DNA was isolated from fecal pellets using DNeasy Blood & Tissue Kit (QIAGEN) according to the manufacturer's protocol. The concentration of DNA isolated from each pellet was obtained via NanoDrop. qPCR was performed using PowerUp SYBR Green Master Mix according to the manufacturer's protocol (Applied Biosystems, Carlsbad, USA) with primer sets targeting the 16S ribosomal subunit of *L. reuteri* (Forward: 5'-GAAGATCAGTCGCAYTGGCCCAA-3'; Reverse: 5'-TCCATTGTGGCCGATCAG-3') and of general bacteria (Forward: 5'-ACTCCTACGGGAGGCAGCAG-3'; Reverse: 5'-ATTACCGCGGCTGCTGG-3') (Sun et al., 2016). *L. reuteri* and total bacteria levels were calculated from Ct values using a standard

curve and the ratio of *L. reuteri*/total bacterial load was calculated for each mouse. All values were normalized to the average of the WT group to set the WT average equal to 1.

Culture and Treatment with *Lactobacillus reuteri*.—*Lactobacillus reuteri* 6475 was cultured anaerobically in MRS broth at 37°C in a 90% N_2, 5% CO_2, 5% H_2 environment as previously described (Buffington et al., 2016). Briefly, cultures were centrifuged, washed, resuspended in PBS, and frozen at −80°C until use. PBS (vehicle) or *L. reuteri* was added to the drinking water daily to minimize dosage variability. The experimental group received live bacteria (~1×10^8 organisms/mouse/day), while the control group received equal volume of PBS. Mice drank the treated water *ad libitum* during the treatment period. Fecal sample collection, behavioral assays, tissue collection and electrophysiological recordings were initiated 4 weeks after the beginning of the treatment period.

Electrophysiological Recordings.—Recordings were performed as previously described (Buffington et al., 2016; Sgritta et al., 2019). Briefly, animals were anaesthetized with isoflurane and then decapitated. The brain was rapidly removed from the skull and fixed on a vibroslicer stage (VT 1000S, Leica Microsystems, Buffalo Grove, IL) with cyano-acrylic glue. Acute 220–250 μm-thick horizontal slices were cut in ice-cold (2–3°C) cutting-solution containing the following (in mM): 87 NaCl, 25 NaHCO3, 25 glucose, 75 sucrose, 2.5 KCl, 1.25 NaH2PO4, 0.5 CaCl2and 7 MgCl2(equilibrated with 95% O2–5% CO2 gas mixture, pH 7.3–7.5). Slices were incubated in the same cutting solution for 20 minutes at 32°C and then stored at room temperature in a holding bath containing oxygenated standard artificial cerebrospinal fluid (ACSF) containing (in mM): 125 NaCl, 25 NaHCO3, 25 glucose, 2.5 KCl, 1.25 NaH2PO4, 2 CaCl2, and 1 MgCl2(equilibrated with 95% O2–5% CO2), for at least 40 minutes, before being transferred to a recording chamber mounted on the stage of an upright microscope (Examiner D1, Carl Zeiss, Oberkochen, Germany). The slices were perfused with oxygenated ACSF (2 ml/min) containing the GABAA receptor antagonist picrotoxin (100 μM; Sigma-Aldrich, USA) and maintained at 32°C with a Peltier feedback device (TC-324B, Warner Instrument). Recordings were performed with Multiclamp700B (Molecular Devices), sampled at 20 kHz with Digidata 511440A(Molecular Device) interface, filtered online at 3 kHz with a Bessel low-pass filter and analyzed off-line with pClamp10 software (Molecular Devices). Patch pipettes were pulled from borosilicate glass capillaries (World Precision Instruments, Inc., FL) and filled with following intracellular solution (in mM): 117 CsMeSO3, 0.4 EGTA, 20 HEPES, 2.8 NaCl, 2.5 Mg-ATP, and 0.25 Na-GTP; 5 TEA Cl, pH was adjusted to 7.3 and osmolarity to 290 mOsm using a vapor pressure osmometer Vapro5600 (ELITechGroupWescor, South Logan, Utah,USA). When filled with the intracellular solution, patch pipettes had a resistance of 2.0–3.0MΩbefore seal formation. The ventral tegmental area (VTA) was visually identified by infrared differential interference contrast video microscopy and lateral VTA was identified considering the medial lemniscus and the medial terminal nucleus of the accessory optic tract as anatomical landmarks. After establishing a gigaohm seal (>2GΩ) and recording stable spontaneous firing in cell-attached mode, neurons were voltage clamped in whole cell configuration. Dopaminergic (DA) neurons in this area were identified evaluating the following features: 1) cells firing at a frequency of 1–5 Hz and the spike width > 1ms in cell attached configuration, 2) membrane capacitance (Cm) > 28

pF and 3) the presence of an Ih current and a leak current > 150 pA, when hyperpolarized from −40 mV to −120 mVin 10 mV steps (Bariselli et al., 2016; Huang et al., 2016; Zhang et al., 2010). Passive electrode-cell parameters were monitored throughout the experiments, analyzing passive current relaxations induced by 10 mV hyperpolarizing steps applied at the beginning of every trace. Variation of series resistance (Rs) > 20% led to the rejection of the experiment. AMPAR/NMDAR ratios were calculated as previously described (Buffington et al., 2016; Huang et al., 2016; Sgritta et al., 2019) Briefly, neurons were slowly voltage clamped at +40 mV until the holding current stabilized (at 200 pA). Excitatory post synaptic currents (EPSCs) were evoked at 0.05 Hz with a bipolar stimulating electrode placed 50–150 μm rostral to the lateral VTA. After recording the dual-component EPSCs, DL-AP5 (100 μM) was bath-applied for 10 minutes to isolate the AMPAR current, blocking the NMDAR. The NMDAR component was then obtained by offline subtraction of the AMPAR component from the original EPSC. The peak amplitudes of the isolated components were used to calculate the AMPAR/NMDAR ratios. Cocaine hydrochloride (Sigma-Aldrich, St. Louis, MO) was dissolved in 0.9% saline and injected intra peritoneally (I.P.) at a volume of 5 ml/kg 24 hours prior to electrophysiological recordings.

To analyze the miniature excitatory post synaptic currents (mEPSCs) in the medial prefrontal cortex (mPFC), coronal sections of mPFC were cut 300 μm thick. Patch pipettes were filled with a solution containing (in mM) 110 K-gluconate, 10 KCI, 10 HEPES, 10 Na_2-phosphocreatine, 2 Mg_3-ATP, and 0.2 Na_3-GTP. When filled with the internal solution, patch pipettes had a resistance of 3–5 mΩ before seal formation. L2/3 neurons of the mPFC were identified under visual guidance and were clamped at −70 mV. mEPSCs were recorded with a background activity protocol, in the presence of 100 μM picrotoxin and of 1 μM TTX. Recordings were low-pass filtered at 2 Hz and sampled at 20 kHz and analyzed off-line with pClamp10 software. All spontaneous currents were digitally filtered at 1.5 kHz and analyzed off-line. Automated mEPSC analysis was performed with Clampfit software. A further visual inspection of detected signals allowed us to reject noise artifacts. A period of 5 min was used to evaluate mEPSC frequency and mEPSC amplitude.

Immunofluorescence.—Immunofluorescence was performed as previously described (Buffington et al., 2016; Sgritta et al., 2019). Mice were deeply anesthetized by inhalation of isoflurane and perfused transcardially with 10 mL 0.9% PBS followed by 30 mL 4% paraformaldehyde (PFA) in 0.1M phosphate buffer (PFA). Brains were post-fixed in 4% PFA at 4°C overnight, then cryoprotected in 30% sucrose 0.1M PB over 3 days. Coronal slices (30 μm) thick were obtained from frozen tissue using a sliding blade microtome then transferred to ice cold PBS. Slices were blocked with 5% normal goat serum, 0.3% Triton X-100 0.1M PB (PBTgs) for 1 hour rocking at room temperature (RT) and then incubated in primary antibodies [rabbit anti-oxytocin, ImmunoStar #20068 (1:2,000 dilution); mouse anti-NeuN, Millipore, #MAB377 (1:2,000 dilution] diluted in PBTgs rocking at 4°C for 24 hr. Slices were then washed three times with 0.3% Triton X-100 0.1M PB. Primary antibodies were visualized using secondary goat anti-rabbit Alexa Fluor 488 (ThermoFisher Scientific, #A-11034) and goat anti-mouse Alexa Fluor 594 (ThermoFisher Scientific, #A-11032) antibodies (1:1,000 dilution). Slices were incubated in secondary antibodies rocking in the dark for 1 hr at RT. Five minute final washes with each of PBTgs, 0.1M

PB, and 0.05M PB preceded mounting onto 2% gelatin (Sigma-Aldrich, #G9391)-coated coverslips. Nuclei were visualized using Vectashield H-1200 with DAPI (Vector Labs, #H-1200).

Fluorescent imaging and data acquisition were performed on a Zeiss AxioImager.Z2 microscope (Carl Zeiss MicroImaging) mounted with an AxioCam digital camera (Carl Zeiss MicroImaging). Images were captured using AxioVision acquisition software (Carl Zeiss Microimaging). All images within a given dataset were acquired at identical exposure times, within a given channel, to allow comparison of signal intensity. In some images, contrast and brightness were linearly adjusted using Photoshop (Adobe). Image processing was applied uniformly across all images within a given dataset. Fluorescence intensity was measured in ImageJ (NIH) by selecting regions of interest (Oxytocin- and NeuN-positive hypothalamic cell bodies). Hypothalamic oxytocin+ and NeuN+ cell number was assessed in ImageJ using the following operational sequence: (i) open image file, (ii) subtract background, (iii) adjust threshold, (iv) convert to mask, (v) watershed, (vi) analyze particles. Automatic identification of cell boundaries was validated against the source image by an experimenter blind to group allocation.

Oxytocin Administration.—Oxytocin (Tocris Bioscience) was administrated intranasally at a dose of 200 μg/kg as previously reported (Buffington et al., 2016; Sgritta et al., 2019). Briefly, oxytocin was dissolved in 10% dimethyl sulfoxide (DMSO)/90% PBS. 10% DMSO/90% PBS was used as the vehicle control. 1.25 μL of vehicle or oxytocin were administrated into each nostril from a P10 pipette 30 minutes prior to social behavior testing, since the effects of oxytocin last 2 hours with this delivery method (Peñagarikano et al., 2015).

Metabolomic Profiling.—Fecal samples were collected from mice in sterile microcentrifuge tubes, frozen immediately on dry ice, and stored at −80°C until processing. Samples were prepared using the automated MicroLab STAR system (Hamilton Co.) and analyzed using ultrahigh performance liquid chromatography-tandem mass spectrometry (UPLC-MS/MS) on a Waters (Milford, MA) ACQUITY ultra-performance liquid chromatography (UPLC) and a Thermo Scientific Q-Exactive high resolution/accurate mass spectrometer interfaced with a heated electrospray ionization (HESI-II) source and Orbitrap mass analyzer operated at 35,000 mass resolution by Metabolon Inc. (Durham, North Carolina). Overall, 752 known compounds were identified by comparing profiles to a known metabolomic library using the Metabolon LIMS system. Values were normalized in terms of raw area count and each biochemical was rescaled to set the median equal to 1 across all three groups. Missing values were imputed, being set to the lowest observed value for each metabolite.

Tetrahydrobiopterin (BH4) Administration.—(6R)-5,6,7,8-Tetrahydrobiopterin dihydrochloride (BH4, Sigma-Aldrich #T4425) was administered *via* oral gavage at a dose of 20 mg/kg. Briefly, BH4 was dissolved (5 mg/mL) in anaerobic water under anaerobic conditions (90% N_2, 5% CO_2, 5% H_2 environment) to prevent oxidation. Aliquots were frozen at −80°C until use. Mice were gavaged with either vehicle or BH4 daily for 2–4 weeks and 2 hours prior to behavior tests.

Oxytocin Receptor Antagonist Administration.—L-371,257 (Tocris Bioscience) was administrated intranasally at a dose of ~300 μg/kg, as previously reported (Peñagarikano et al., 2015). Briefly, L-371,257 was dissolved in 10% dimethyl sulfoxide (DMSO) in PBS and 10% DMSO in PBS was used as the vehicle control. Two microliters of L-371,257 (or vehicle) were administrated into each nostril 20 minutes prior to reciprocal social interaction test.

SPRi3 Administration.—SPRi3 (Tocris Bioscience) was administered intraperitoneally (I.P.) at a dose of 300 mg/kg based on previous reports (Cronin et al., 2018; Latremoliere et al., 2015). SPRi3 was dissolved in 50% w/v 2-hydroxypropyl-β-cyclodextrin (Sigma Life Sciences) in 0.9% sterile saline and 50% w/v 2-hydroxypropyl-β-cyclodextrin in 0.9% sterile saline was used as the vehicle control. Mice were injected every other day for 5 days prior to behavior and 1 hour prior to behavioral tests.

QUANTIFICATION AND STATISTICAL ANALYSIS.

Data were presented as mean ± SEM with individual data points also shown. Statistical analyses performed include Mann-Whitney *U* test, student t-test, one- or two-way ANOVA with Bonferroni post hoc analysis to correct for multiple comparisons, unless otherwise indicated. *U*, *t*, *F*, and *P* values were presented in the figure legends. $P < 0.05$ was considered statistically significant. $^{*}P < 0.05$, $^{**}P < 0.01$, $^{***}P < 0.001$, $^{****}P < 0.0001$. GraphPad's Prism (La Jolla, CA) software was used to perform statistical analyses for behavioral and electrophysiological experiments and to generate graphical data representations.

The analyses for metabolomics were conducted in RStudio 1.1.463 using R 3.3.3. The hierarchical clustering of the samples was determined using pvclust (Suzuki and Shimodaira, 2006) by generating a stable dendrogram with selective inference (SI) P-values after bootstrapping across 1000 permutations. SI values > 95% can be considered certain and significant. The heatmap was then constructed and visualized using the heatmap.2 function in gplots (version 3.0.1.1). Random forest analysis was performed using the randomForest function in the randomForest package (version 4.6–14) and visualized using the ggplot function in the ggplot2 package (version 3.2.0).

The analyses for the 16S rRNA gene sequencing were conducted in RStudio 1.2.1335 using R 3.6.0. Beta diversity analyses were performed using two strategies. In the first, sequence abundances were analyzed using the phylogenetic isometric log transform [PhILR, R package version 1.10.1 (Silverman et al., 2017)] and the Euclidean distance between transformed values for each sample. In the second, Bray-Curtis and Unifrac dissimilarities were calculated using the R package phyloseq v1.28.0 (McMurdie and Holmes, 2013). Beta diversity PERMANOVA hypothesis testing was performed for all dissimilarity metrics using the *adonis* function in the R package vegan v2.5–6 (Oksanen et al., 2019), adjusting for sex, cage, and/or time covariates where applicable. No significant differences in dispersion were observed that were consistent across dissimilarity metrics as measured using the *betadisper* function in the R package vegan v2.5–6 (data not shown). Alpha-diversity indices were calculated using phyloseq, after subsampling sequence variant tables to the minimum number of reads assigned to a sample in a given experiment. Hypothesis testing for alpha-

diversity metrics was performed using the breakaway package v4.7.2 for richness estimates (Willis et al., 2020), and using linear mixed models for the Shannon index. Differential abundance analysis of sequence variants and PICRUSt2-inferred MetaCyc pathways was performed using the aldex.glm function in the ALDEx2 package version 1.16.0 (Fernandes et al., 2014) with default parameters, again adjusting for applicable covariates. Features with a Benjamini-Hochberg FDR-corrected p-value less than 0.05 were considered significant (Benjamini et al., 2001). Visualizations of microbiome data were generated using the ggplot2 (v3.3.2) and ggtree (v1.16.6) packages.

Supplementary Material

Refer to Web version on PubMed Central for supplementary material.

ACKNOWLEDGEMENTS:

We thank Marina Grasso for administrative support, Alton Swennes, Stephanie Fowler, and Angela Mannone for veterinary support, Kristi Hoffman and Umesh Karandikar for sequencing support, and Jacqunae Mays and other members of the Costa-Mattioli lab for comments on the manuscript.

Funding: This work was supported by funding from NIH (R01 MH112356; R01 HL122593; R01 DK114034, 2T32AI060537–16) and the generous support from Sammons Enterprise to M.C.-M. P.J.T. is a Nadia's Gift Foundation Innovator supported, in part, by the Damon Runyon Cancer Research Foundation (DRR-42–16).

REFERENCES

American Psychiatric Association (2013). Diagnostic and statistical manual of mental disorders (DSM-5®) (American Psychiatric Pub).

Ang QY, Alexander M, Newman JC, Tian Y, Cai J, Upadhyay V, Turnbaugh JA, Verdin E, Hall KD, Leibel RL, et al. (2020). Ketogenic Diets Alter the Gut Microbiome Resulting in Decreased Intestinal Th17 Cells. Cell 181, 1263–1275.e1216. [PubMed: 32437658]

Bakkaloglu B, O'Roak BJ, Louvi A, Gupta AR, Abelson JF, Morgan TM, Chawarska K, Klin A, Ercan-Sencicek AG, Stillman AA, et al. (2008). Molecular Cytogenetic Analysis and Resequencing of Contactin Associated Protein-Like 2 in Autism Spectrum Disorders. The American Journal of Human Genetics 82, 165–173. [PubMed: 18179895]

Barbera P, Kozlov AM, Czech L, Morel B, Darriba D, Flouri T, and Stamatakis A (2019). EPA-ng: Massively Parallel Evolutionary Placement of Genetic Sequences. Systematic Biology 68, 365–369. [PubMed: 30165689]

Bariselli S, Hörnberg H, Prévost-Solié C, Musardo S, Hatstatt-Burklé L, Scheiffele P, and Bellone C (2018). Role of VTA dopamine neurons and neuroligin 3 in sociability traits related to nonfamiliar conspecific interaction. Nature Communications 9, 3173.

Bariselli S, Tzanoulinou S, Glangetas C, Prevost-Solie C, Pucci L, Viguie J, Bezzi P, O'Connor EC, Georges F, Luscher C, et al. (2016). SHANK3 controls maturation of social reward circuits in the VTA. Nat Neurosci 19, 926–934. [PubMed: 27273769]

Benjamini Y, Drai D, Elmer G, Kafkafi N, and Golani I (2001). Controlling the false discovery rate in behavior genetics research. Behav Brain Res 125, 279–284. [PubMed: 11682119]

Benson AK, Kelly SA, Legge R, Ma F, Low SJ, Kim J, Zhang M, Oh PL, Nehrenberg D, Hua K, et al. (2010). Individuality in gut microbiota composition is a complex polygenic trait shaped by multiple environmental and host genetic factors. Proc Natl Acad Sci U S A 107, 18933–18938. [PubMed: 20937875]

Bolyen E, Rideout JR, Dillon MR, Bokulich NA, Abnet CC, Al-Ghalith GA, Alexander H, Alm EJ, Arumugam M, Asnicar F, et al. (2019). Reproducible, interactive, scalable and extensible microbiome data science using QIIME 2. Nature Biotechnology 37, 852–857.

Buffington SA, Di Prisco GV, Auchtung TA, Ajami NJ, Petrosino JF, and Costa-Mattioli M (2016). Microbial Reconstitution Reverses Maternal Diet-Induced Social and Synaptic Deficits in Offspring. Cell 165, 1762–1775. [PubMed: 27315483]

Callahan BJ, McMurdie PJ, Rosen MJ, Han AW, Johnson AJA, and Holmes SP (2016). DADA2: High-resolution sample inference from Illumina amplicon data. Nature Methods 13, 581–583. [PubMed: 27214047]

Caporaso JG, Lauber CL, Walters WA, Berg-Lyons D, Lozupone CA, Turnbaugh PJ, Fierer N, and Knight R (2011). Global patterns of 16S rRNA diversity at a depth of millions of sequences per sample. Proceedings of the National Academy of Sciences 108, 4516.

Carter MD, Shah CR, Muller CL, Crawley JN, Carneiro AMD, and Veenstra-VanderWeele J (2011). Absence of preference for social novelty and increased grooming in integrin β3 knockout mice: initial studies and future directions. Autism Res 4, 57–67. [PubMed: 21254450]

Caspi R, Billington R, Keseler IM, Kothari A, Krummenacker M, Midford PE, Ong WK, Paley S, Subhraveti P, and Karp PD (2020). The MetaCyc database of metabolic pathways and enzymes - a 2019 update. Nucleic Acids Research 48, D445–D453. [PubMed: 31586394]

Chen C-J, Sgritta M, Mays J, Zhou H, Lucero R, Park J, Wang IC, Park JH, Kaipparettu BA, Stoica L, et al. (2019). Therapeutic inhibition of mTORC2 rescues the behavioral and neurophysiological abnormalities associated with Pten-deficiency. Nature Medicine 25, 1684–1690.

Ciosek J, and Guzek JW (1992). Neurohypophysial function and pteridines: effect of (6R)-5,6,7,8-tetrahydro-alpha-biopterin on bioassayed hypothalamo-neurohypophysial vasopressin and oxytocin in the rat. Folia Med Cracov 33, 25–35. [PubMed: 1342998]

Ciosek J, Guzek JW, and Orlowska-Majdak M (1992). Neurohypophysial vasopressin and oxytocin as influenced by (6R)-5,6,7,8-tetrahydro-alpha-biopterin in euhydrated and dehydrated rats. Biol Chem Hoppe Seyler 373, 1079–1083. [PubMed: 1418678]

Cronin SJF, Seehus C, Weidinger A, Talbot S, Reissig S, Seifert M, Pierson Y, McNeill E, Longhi MS, Turnes BL, et al. (2018). The metabolite BH4 controls T cell proliferation in autoimmunity and cancer. Nature 563, 564–568. [PubMed: 30405245]

Czech L, Barbera P, and Stamatakis A (2020). Genesis and Gappa: processing, analyzing and visualizing phylogenetic (placement) data. Bioinformatics 36, 3263–3265. [PubMed: 32016344]

De Angelis M, Piccolo M, Vannini L, Siragusa S, De Giacomo A, Serrazzanetti DI, Cristofori F, Guerzoni ME, Gobbetti M, and Francavilla R (2013). Fecal microbiota and metabolome of children with autism and pervasive developmental disorder not otherwise specified. PLoS One 8, e76993. [PubMed: 24130822]

Desbonnet L, Clarke G, Shanahan F, Dinan TG, and Cryan JF (2014). Microbiota is essential for social development in the mouse. Mol Psychiatry 19, 146–148. [PubMed: 23689536]

Donaldson ZR, and Young LJ (2008). Oxytocin, vasopressin, and the neurogenetics of sociality. Science 322, 900–904. [PubMed: 18988842]

Douglas GM, Maffei VJ, Zaneveld JR, Yurgel SN, Brown JR, Taylor CM, Huttenhower C, and Langille MGI (2020). PICRUSt2 for prediction of metagenome functions. Nature Biotechnology 38, 685–688.

Elinav E, Strowig T, Kau AL, Henao-Mejia J, Thaiss CA, Booth CJ, Peaper DR, Bertin J, Eisenbarth SC, Gordon JI, et al. (2011). NLRP6 inflammasome regulates colonic microbial ecology and risk for colitis. Cell 145, 745–757. [PubMed: 21565393]

Fernandes AD, Reid JNS, Macklaim JM, McMurrough TA, Edgell DR, and Gloor GB (2014). Unifying the analysis of high-throughput sequencing datasets: characterizing RNA-seq, 16S rRNA gene sequencing and selective growth experiments by compositional data analysis. Microbiome 2, 15. [PubMed: 24910773]

Finegold SM, Dowd SE, Gontcharova V, Liu C, Henley KE, Wolcott RD, Youn E, Summanen PH, Granpeesheh D, Dixon D, et al. (2010). Pyrosequencing study of fecal microflora of autistic and control children. Anaerobe 16, 444–453. [PubMed: 20603222]

Fischbach Michael A., and Segre Julia A. (2016). Signaling in Host-Associated Microbial Communities. Cell 164, 1288–1300. [PubMed: 26967294]

Goodrich JK, Waters JL, Poole AC, Sutter JL, Koren O, Blekhman R, Beaumont M, Van Treuren W, Knight R, Bell JT, et al. (2014). Human genetics shape the gut microbiome. Cell 159, 789–799. [PubMed: 25417156]

Gunaydin Lisa A., Grosenick L, Finkelstein Joel C., Kauvar Isaac V., Fenno Lief E., Adhikari A, Lammel S, Mirzabekov Julie J., Airan Raag D., Zalocusky Kelly A., et al. (2014). Natural Neural Projection Dynamics Underlying Social Behavior. Cell 157, 1535–1551. [PubMed: 24949967]

Holmdahl R, and Malissen B (2012). The need for littermate controls. Eur J Immunol 42, 45–47. [PubMed: 22213045]

Hsiao EY, McBride SW, Hsien S, Sharon G, Hyde ER, McCue T, Codelli JA, Chow J, Reisman SE, Petrosino JF, et al. (2013). Microbiota modulate behavioral and physiological abnormalities associated with neurodevelopmental disorders. Cell 155, 1451–1463. [PubMed: 24315484]

Huang W, Placzek AN, Viana Di Prisco G, Khatiwada S, Sidrauski C, Krnjevic K, Walter P, Dani JA, and Costa-Mattioli M (2016). Translational control by eIF2alpha phosphorylation regulates vulnerability to the synaptic and behavioral effects of cocaine. Elife 5.

Huang W-C, Zucca A, Levy J, and Page DT (2020). Social Behavior Is Modulated by Valence-Encoding mPFC-Amygdala Sub-circuitry. Cell Reports 32, 107899. [PubMed: 32668253]

Huang Y-C, and Hessler NA (2008). Social Modulation during Songbird Courtship Potentiates Midbrain Dopaminergic Neurons. PLoS One 3, e3281. [PubMed: 18827927]

Human Microbiome Project C (2012). Structure, function and diversity of the healthy human microbiome. Nature 486, 207–214. [PubMed: 22699609]

Hung LW, Neuner S, Polepalli JS, Beier KT, Wright M, Walsh JJ, Lewis EM, Luo L, Deisseroth K, Dolen G, et al. (2017). Gating of social reward by oxytocin in the ventral tegmental area. Science 357, 1406–1411. [PubMed: 28963257]

Janssen S, McDonald D, Gonzalez A, Navas-Molina JA, Jiang L, Xu ZZ, Winker K, Kado DM, Orwoll E, Manary M, et al. (2018). Phylogenetic Placement of Exact Amplicon Sequences Improves Associations with Clinical Information. mSystems 3, e00021–00018. [PubMed: 29719869]

Jiang Y. h., and Ehlers Michael D. (2013). Modeling Autism by SHANK Gene Mutations in Mice. Neuron 78, 8–27. [PubMed: 23583105]

Kazdoba TM, Leach PT, Yang M, Silverman JL, Solomon M, and Crawley JN (2016). Translational Mouse Models of Autism: Advancing Toward Pharmacological Therapeutics. In Translational Neuropsychopharmacology, Robbins TW, and Sahakian BJ, eds. (Cham: Springer International Publishing), pp. 1–52.

Khachatryan ZA, Ktsoyan ZA, Manukyan GP, Kelly D, Ghazaryan KA, and Aminov RI (2008). Predominant role of host genetics in controlling the composition of gut microbiota. PLoS One 3, e3064. [PubMed: 18725973]

Klaiman C, Huffman L, Masaki L, and Elliott GR (2013). Tetrahydrobiopterin as a treatment for autism spectrum disorders: a double-blind, placebo-controlled trial. J Child Adolesc Psychopharmacol 23, 320–328. [PubMed: 23782126]

Latremoliere A, Latini A, Andrews N, Cronin Shane J., Fujita M, Gorska K, Hovius R, Romero C, Chuaiphichai S, Painter M, et al. (2015). Reduction of Neuropathic and Inflammatory Pain through Inhibition of the Tetrahydrobiopterin Pathway. Neuron 86, 1393–1406. [PubMed: 26087165]

Lazaro MT, Taxidis J, Shuman T, Bachmutsky I, Ikrar T, Santos R, Marcello GM, Mylavarapu A, Chandra S, Foreman A, et al. (2019). Reduced Prefrontal Synaptic Connectivity and Disturbed Oscillatory Population Dynamics in the CNTNAP2 Model of Autism. Cell reports 27, 2567–2578.e2566. [PubMed: 31141683]

Liu Z-H, and Smith CB (2009). Dissociation of social and nonsocial anxiety in a mouse model of fragile X syndrome. Neuroscience Letters 454, 62–66. [PubMed: 19429055]

LoParo D, and Waldman ID (2015). The oxytocin receptor gene (OXTR) is associated with autism spectrum disorder: a meta-analysis. Molecular Psychiatry 20, 640–646. [PubMed: 25092245]

Louca S, and Doebeli M (2018). Efficient comparative phylogenetics on large trees. Bioinformatics 34, 1053–1055. [PubMed: 29091997]

Lynch JB, and Hsiao EY (2019). Microbiomes as sources of emergent host phenotypes. Science 365, 1405–1409. [PubMed: 31604267]

Margulis L (1993). Origins of species: acquired genomes and individuality. Biosystems 31, 121–125. [PubMed: 8155844]

Mayer EA, Tillisch K, and Gupta A (2015). Gut/brain axis and the microbiota. The Journal of Clinical Investigation 125, 926–938. [PubMed: 25689247]

McMurdie PJ, and Holmes S (2013). phyloseq: an R package for reproducible interactive analysis and graphics of microbiome census data. PLoS One 8, e61217. [PubMed: 23630581]

Melis MR, Melis T, Cocco C, Succu S, Sanna F, Pillolla G, Boi A, Ferri GL, and Argiolas A (2007). Oxytocin injected into the ventral tegmental area induces penile erection and increases extracellular dopamine in the nucleus accumbens and paraventricular nucleus of the hypothalamus of male rats. The European journal of neuroscience 26, 1026–1035. [PubMed: 17672853]

Methé BA, Nelson KE, Pop M, Creasy HH, Giglio MG, Huttenhower C, Gevers D, Petrosino JF, Abubucker S, Badger JH, et al. (2012). A framework for human microbiome research. Nature 486, 215–221. [PubMed: 22699610]

O'Roak BJ, Deriziotis P, Lee C, Vives L, Schwartz JJ, Girirajan S, Karakoc E, Mackenzie AP, Ng SB, Baker C, et al. (2011). Exome sequencing in sporadic autism spectrum disorders identifies severe de novo mutations. Nature genetics 43, 585–589. [PubMed: 21572417]

Oksanen J, Blanchet FG, Friendly M, Kindt R, Pierre L, McGlinn D, Minchin PR, O'Hara RB, Simpson GL, Solymos P, et al. (2019). vegan: Community Ecology Package. R package version 2.5–6.

Olson CA, Vuong HE, Yano JM, Liang QY, Nusbaum DJ, and Hsiao EY (2018). The Gut Microbiota Mediates the Anti-Seizure Effects of the Ketogenic Diet. Cell 174, 497. [PubMed: 30007420]

Peñagarikano O, Abrahams Brett S., Herman Edward I., Winden Kellen D., Gdalyahu A, Dong H, Sonnenblick Lisa I., Gruver R, Almajano J, Bragin A, et al. (2011). Absence of CNTNAP2 Leads to Epilepsy, Neuronal Migration Abnormalities, and Core Autism-Related Deficits. Cell 147, 235–246. [PubMed: 21962519]

Peñagarikano O, Lázaro MT, Lu X-H, Gordon A, Dong H, Lam HA, Peles E, Maidment NT, Murphy NP, Yang XW, et al. (2015). Exogenous and evoked oxytocin restores social behavior in the Cntnap2 mouse model of autism. Science Translational Medicine 7, 271ra278.

Pietropaolo S, Guilleminot A, Martin B, D'Amato FR, and Crusio WE (2011). Genetic-background modulation of core and variable autistic-like symptoms in Fmr1 knock-out mice. PLoS One 6, e17073–e17073. [PubMed: 21364941]

Poliak S, Gollan L, Martinez R, Custer A, Einheber S, Salzer JL, Trimmer JS, Shrager P, and Peles E (1999). Caspr2, a new member of the neurexin superfamily, is localized at the juxtaparanodes of myelinated axons and associates with K+ channels. Neuron 24, 1037–1047. [PubMed: 10624965]

Poliak S, Gollan L, Salomon D, Berglund EO, Ohara R, Ranscht B, and Peles E (2001). Localization of Caspr2 in myelinated nerves depends on axon-glia interactions and the generation of barriers along the axon. J Neurosci 21, 7568–7575. [PubMed: 11567047]

Poliak S, Salomon D, Elhanany H, Sabanay H, Kiernan B, Pevny L, Stewart CL, Xu X, Chiu SY, Shrager P, et al. (2003). Juxtaparanodal clustering of Shaker-like K+ channels in myelinated axons depends on Caspr2 and TAG-1. J Cell Biol 162, 1149–1160. [PubMed: 12963709]

Poutahidis T, Kearney SM, Levkovich T, Qi P, Varian BJ, Lakritz JR, Ibrahim YM, Chatzigiagkos A, Alm EJ, and Erdman SE (2013). Microbial symbionts accelerate wound healing via the neuropeptide hormone oxytocin. PloS one 8, e78898. [PubMed: 24205344]

Quast C, Pruesse E, Yilmaz P, Gerken J, Schweer T, Yarza P, Peplies J, and Glockner FO (2013). The SILVA ribosomal RNA gene database project: improved data processing and web-based tools. Nucleic Acids Res 41, D590–596. [PubMed: 23193283]

Rehman A, Sina C, Gavrilova O, Hasler R, Ott S, Baines JF, Schreiber S, and Rosenstiel P (2011). Nod2 is essential for temporal development of intestinal microbial communities. Gut 60, 1354–1362. [PubMed: 21421666]

Ridaura VK, Faith JJ, Rey FE, Cheng J, Duncan AE, Kau AL, Griffin NW, Lombard V, Henrissat B, Bain JR, et al. (2013). Gut microbiota from twins discordant for obesity modulate metabolism in mice. Science 341, 1241214. [PubMed: 24009397]

Rosenberg E, Koren O, Reshef L, Efrony R, and Zilber-Rosenberg I (2007). The role of microorganisms in coral health, disease and evolution. Nature Reviews Microbiology 5, 355–362. [PubMed: 17384666]

Sahin M, and Sur M (2015). Genes, circuits, and precision therapies for autism and related neurodevelopmental disorders. Science 350, aab3897. [PubMed: 26472761]

Sgritta M, Dooling SW, Buffington SA, Momin EN, Francis MB, Britton RA, and Costa-Mattioli M (2019). Mechanisms Underlying Microbial-Mediated Changes in Social Behavior in Mouse Models of Autism Spectrum Disorder. Neuron 101, 246–259 e246. [PubMed: 30522820]

Sharon G, Sampson TR, Geschwind DH, and Mazmanian SK (2016). The Central Nervous System and the Gut Microbiome. Cell 167, 915–932. [PubMed: 27814521]

Sherwin E, Bordenstein SR, Quinn JL, Dinan TG, and Cryan JF (2019). Microbiota and the social brain. Science 366.

Silva AJ, and Ehninger D (2009). Adult reversal of cognitive phenotypes in neurodevelopmental disorders. J Neurodev Disord 1, 150–157. [PubMed: 19812701]

Silverman JD, Washburne AD, Mukherjee S, and David LA (2017). A phylogenetic transform enhances analysis of compositional microbiota data. eLife 6, e21887. [PubMed: 28198697]

Silverman JL, Yang M, Lord C, and Crawley JN (2010). Behavioural phenotyping assays for mouse models of autism. Nat Rev Neurosci 11, 490–502. [PubMed: 20559336]

Stappenbeck TS, and Virgin HW (2016). Accounting for reciprocal host-microbiome interactions in experimental science. Nature 534, 191–199. [PubMed: 27279212]

Strati F, Cavalieri D, Albanese D, De Felice C, Donati C, Hayek J, Jousson O, Leoncini S, Renzi D, Calabro A, et al. (2017). New evidences on the altered gut microbiota in autism spectrum disorders. Microbiome 5, 24. [PubMed: 28222761]

Sun J, Qiao Y, Qi C, Jiang W, Xiao H, Shi Y, and Le GW (2016). High-fat-dieti-nduced obesity is associated with decreased antiinflammatory Lactobacillus reuteri sensitive to oxidative stress in mouse Peyer's patches. Nutrition 32, 265–272. [PubMed: 26620713]

Suzuki R, and Shimodaira H (2006). Pvclust: an R package for assessing the uncertainty in hierarchical clustering. Bioinformatics 22, 1540–1542. [PubMed: 16595560]

Tabouy L, Getselter D, Ziv O, Karpuj M, Tabouy T, Lukic I, Maayouf R, Werbner N, Ben-Amram H, Nuriel-Ohayon M, et al. (2018). Dysbiosis of microbiome and probiotic treatment in a genetic model of autism spectrum disorders. Brain, behavior, and immunity.

Thony B, Auerbach G, and Blau N (2000). Tetrahydrobiopterin biosynthesis, regeneration and functions. Biochem J 347 Pt 1, 1–16. [PubMed: 10727395]

Vuong HE, and Hsiao EY (2017). Emerging Roles for the Gut Microbiome in Autism Spectrum Disorder. Biological psychiatry 81, 411–423. [PubMed: 27773355]

Vuong HE, Yano JM, Fung TC, and Hsiao EY (2017). The Microbiome and Host Behavior. Annual review of neuroscience 40, 21–49.

Willis A, Martin BD, Trinh P, Barger K, and Bunge J (2020). breakaway: Species Richness Estimation and Modeling. R package version 4.7.2.

Xiao L, Priest MF, Nasenbeny J, Lu T, and Kozorovitskiy Y (2017). Biased Oxytocinergic Modulation of Midbrain Dopamine Systems. Neuron 95, 368–384.e365. [PubMed: 28669546]

Ye Y, and Doak TG (2009). A Parsimony Approach to Biological Pathway Reconstruction/Inference for Genomes and Metagenomes. PLOS Computational Biology 5, e1000465. [PubMed: 19680427]

Zhang TA, Placzek AN, and Dani JA (2010). In vitro identification and electrophysiological characterization of dopamine neurons in the ventral tegmental area. Neuropharmacology 59, 431–436. [PubMed: 20600174]

Highlights

- Host genetics & microbiota differentially regulate behaviors in an ASD mouse model
- Microbe therapy (*L. reuteri*) rescues *Cntnap2*$^{-/-}$ social deficits but not hyperactivity
- Microbe-induced metabolite (BH4) selectively rescues *Cntnap2*$^{-/-}$ social deficits
- *L. reuteri* & BH4 improves *Cntnap2*$^{-/-}$ social reward-mediated synaptic transmission

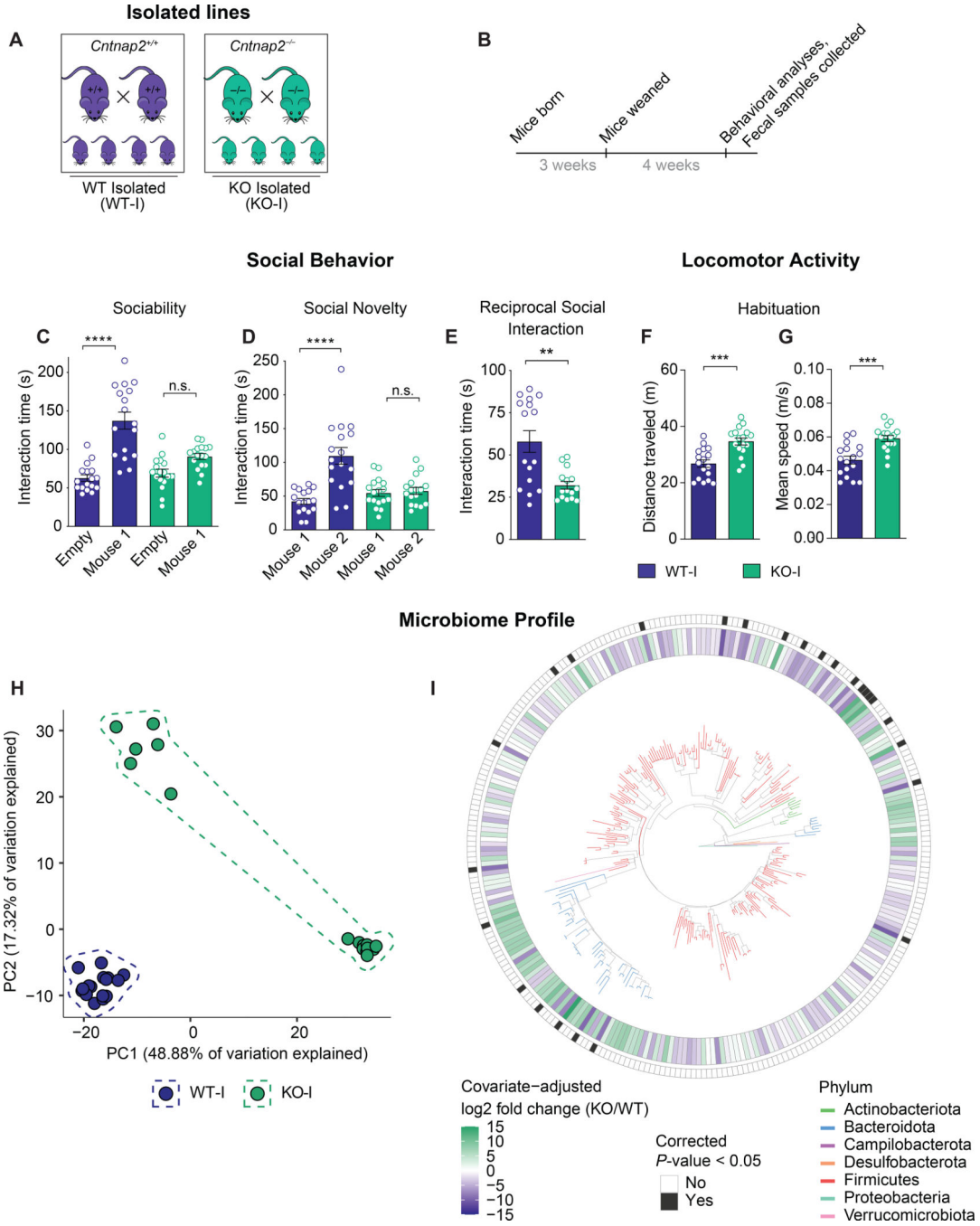

Fig. 1. *Cntnap2*$^{-/-}$ mice generated from isolated breeding lines exhibit impaired social behavior, hyperactivity, and a distinct microbiome composition compared to WT controls.

A, Breeding scheme for the isolated lines (*Cntnap2*$^{+/+}$: WT-I; *Cntnap2*$^{-/-}$: KO-I). **B**, Experimental design for animals from isolated lines. **C-D**, Social behavior in WT-I and KO-I mice as assessed in the 3-chamber test ($n = 17$ per group; **C**, Sociability: WT-I: $t = 7.508$, $P < 0.0001$; KO-I: $t = 1.01$, $P = 0.6322$; two-way ANOVA: $F_{1,64} = 21.11$, $P < 0.0001$; **D**, Social Novelty: WT-I: $t = 6.386$, $P < 0.0001$; KO-I: $t = 0.2782$, $P > 0.9999$; two-way ANOVA, $F_{1,64} = 18.65$, $P < 0.0001$). **E**, Social behavior in WT-I and KO-I mice as assessed

in the reciprocal social interaction test (n = 15–16 per group, Mann-Whitney $U = 52.50$, $P = 0.0065$). **F-G**, Locomotor activity levels in WT-I and KO-I mice as assessed in the habituation phase of the 3-chamber test ($n = 17$ per group; **F**, Distance traveled: WT-I vs KO-I: Mann-Whitney $U = 42$, $P = 0.0002$; **G**, Mean Speed: WT-I vs KO-I: Mann-Whitney $U = 42.5$, $P = 0.0002$). **H**, Beta diversity of the 16S rRNA gene sequencing dataset from feces of WT-I and KO-I mice (n = 16 per group) as determined by principal components analysis (PCA) of PhILR-transformed Euclidean distances (PERMANOVA: $R^2 = 0.35732$, $P = 0.0002$). **I**, Phylogenetic tree of ASVs detected in the 16S rRNA gene sequencing dataset with tree branch colors associated with the phylum of the ASV, the inner circle representing differences in ASV abundance between groups (sliding scale: green = higher in KO, white = no difference, purple = higher in WT), and the outer circle representing the significance level after Benjamini-Hochberg false discovery rate correction (white: not significant, $P \geq 0.05$; black: significant, $P < 0.05$). See also Figure S1 **and** Table S1, S2.

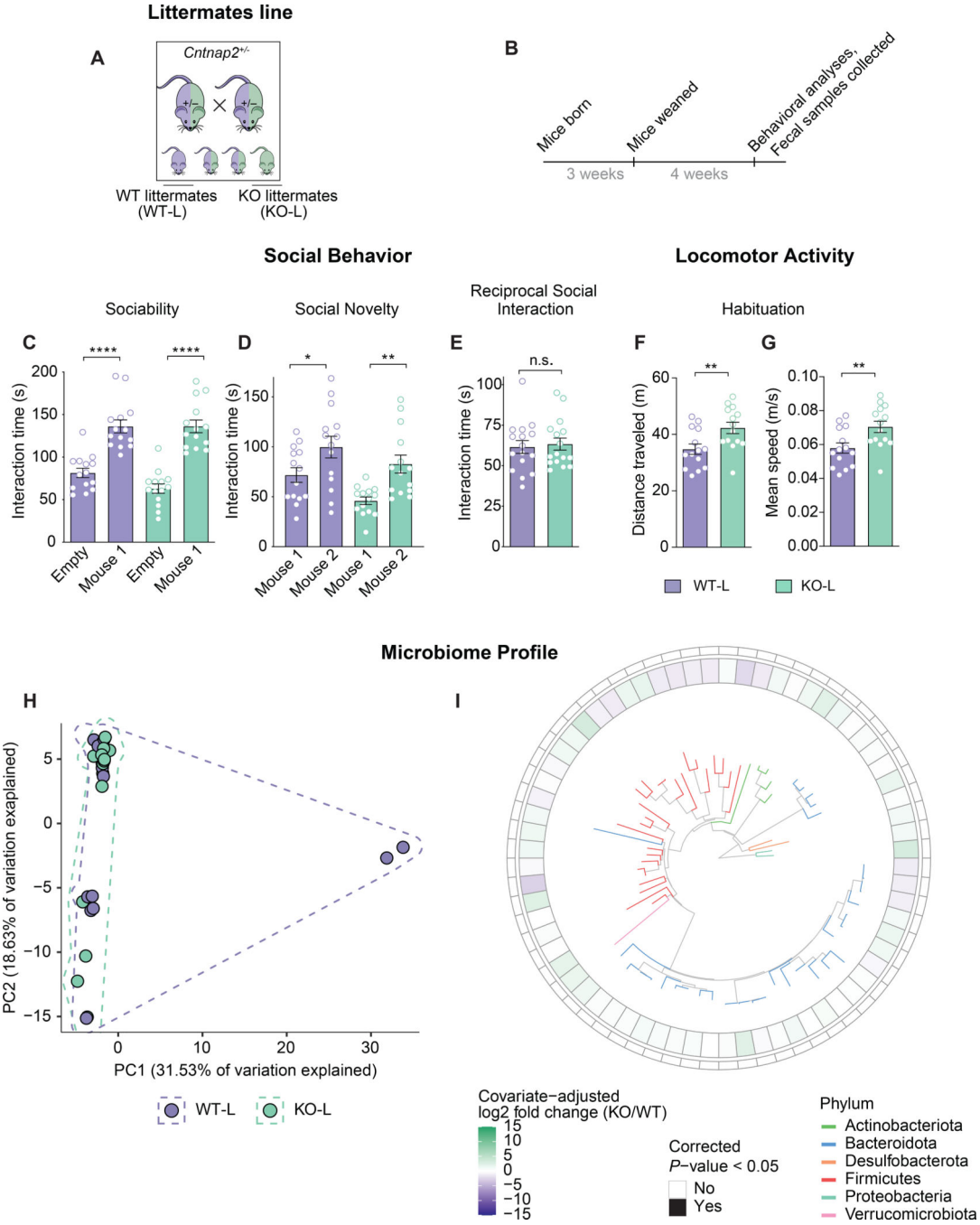

Fig 2. *Cntnap2*$^{-/-}$ mice generated from littermates breeding line exhibit normal social behavior and a microbiome composition similar to WT controls, but remain hyperactive.

A, Breeding scheme for the littermate line (*Cntnap2*$^{+/+}$: WT-L; *Cntnap2*$^{-/-}$: KO-L). **B**, Experimental design for animals from littermate line. **C-D**, Social behavior in WT-L and KO-L mice as assessed in the 3-chamber test ($n = 14$ per group; **C**, Sociability: WT-L: $t = 5.856$, $P < 0.0001$; KO-L: $t = 7.849$, $P < 0.0001$; two-way ANOVA: $F_{1,52} = 1.938$, $P < 0.1650$; **D**, Social Novelty: WT-L: $t = 2.415$, $P = 0.0386$; KO-L: $t = 3.145$, $P = 0.0055$; two-way ANOVA, $F_{1,52} = 0.266$, $P = 0.6082$). **E**, Social behavior in WT-L and KO-L mice

as assessed in the reciprocal social interaction test (n = 16 per group, Mann-Whitney U = 124, P = 0.897)**. F-G**, Locomotor activity levels in WT-L and KO-L mice as assessed in the habituation phase of the 3-chamber test (n = 14 per group; **F**, Distance traveled: WT-L vs KO-L: Mann-Whitney U = 42, P = 0.0091; **G**, Mean speed: WT-L vs KO-L: Mann-Whitney U = 42.5, P = 0.0095). **H**, Beta diversity of the 16S rRNA gene sequencing dataset from feces of WT-L and KO-L mice (n = 14 per group) as determined by principal components analysis (PCA) of PhILR-transformed Euclidean distances (PERMANOVA: R^2 = 0.04440, P = 0.26975). **I**, Phylogenetic tree of ASVs detected in the 16S rRNA gene sequencing dataset with tree branch colors associated with the phylum of the ASV, the inner circle representing differences in ASV abundance between groups (sliding scale: green = higher in KO, white = no difference, purple = higher in WT), and the outer circle representing the significance level after Benjamini-Hochberg false discovery rate correction (white: not significant, $P \geq 0.05$; black: significant, $P < 0.05$). See also Figure S1, and Table S1, S2.

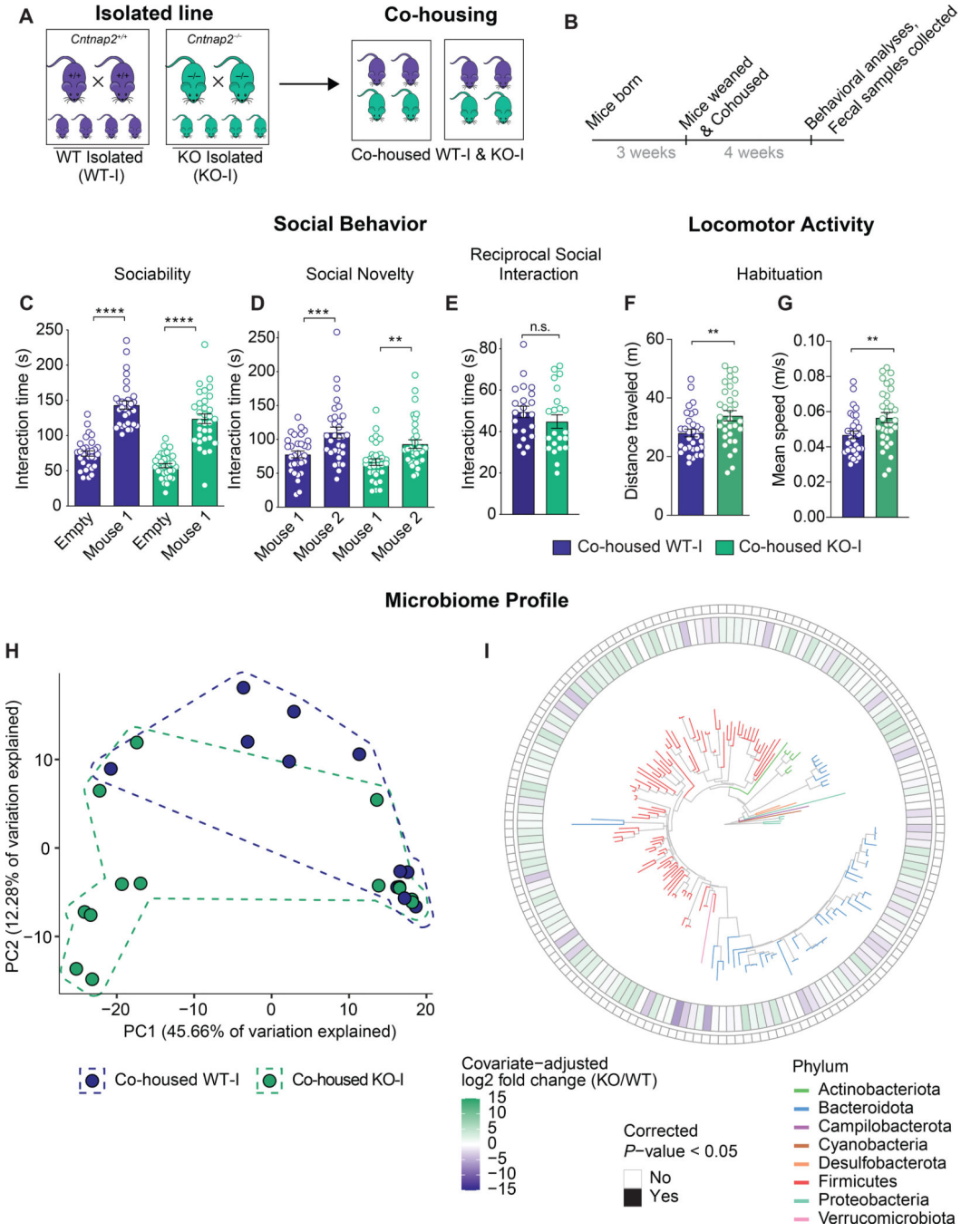

Fig. 3. Co-housing reverses the social deficits and leads to a more similar gut microbiome composition but fails to rescue hyperactivity of KO-I mice.

A-B, Schemes of experimental design. **C-D**, Social behavior in the co-housed WT-I and co-housed KO-I mice as assessed in the 3-chamber test (n = 31–32 per group; **C**, Sociability: co-housed WT-I: t = 9.442, P < 0.0001; co-housed KO-I: t = 9.284, P < 0.0001; two-way ANOVA: $F_{1,122}$ = 0.04696, P = 0.8288; **D**, Social Novelty: co-housed WT-I: t = 3.666, P = 0.0007; co-housed KO-I: t =3.066, P = 0.0053; two-way ANOVA, $F_{1,122}$ = 0.2135, P = 0.6448). **E**, Social behavior in the co-housed WT-I and co-housed KO-I mice as assessed in

the reciprocal social interaction test (n = 22 per group; co-housed WT-I vs co-housed KO-I: Mann-Whitney U = 192, P = 0.2456). **F-G**, Locomotor activity levels of the co-housed WT-I and co-housed KO-I mice as assessed in the habituation phase of the 3-chamber test (n = 31–32 per group; **F**, Distance traveled: co-housed WT-I vs co-housed KO-I: Mann-Whitney U = 307, P = 0.0089; **G**, Mean speed: co-housed WT-I vs co-housed KO-I: Mann-Whitney U = 303, P = 0.0074). **H**, Beta diversity of the 16S rRNA gene sequencing dataset from feces of co-housed WT-I and KO-I mice (n = 12–13 per group) as determined by principal components analysis (PCA) of PhILR-transformed Euclidean distances (PERMANOVA: R^2 = 0.11351, P = 0.04459). **I**, Phylogenetic tree of ASVs detected in the 16S rRNA gene sequencing dataset with tree branch colors associated with the phylum of the ASV, the inner circle representing differences in ASV abundance between groups (sliding scale: green = higher in KO, white = no difference, purple = higher in WT), and the outer circle representing the significance level after Benjamini-Hochberg false discovery rate correction (white: not significant, $P \geq 0.05$; black: significant, $P < 0.05$). See also Figure S2, and Table S1, S2.

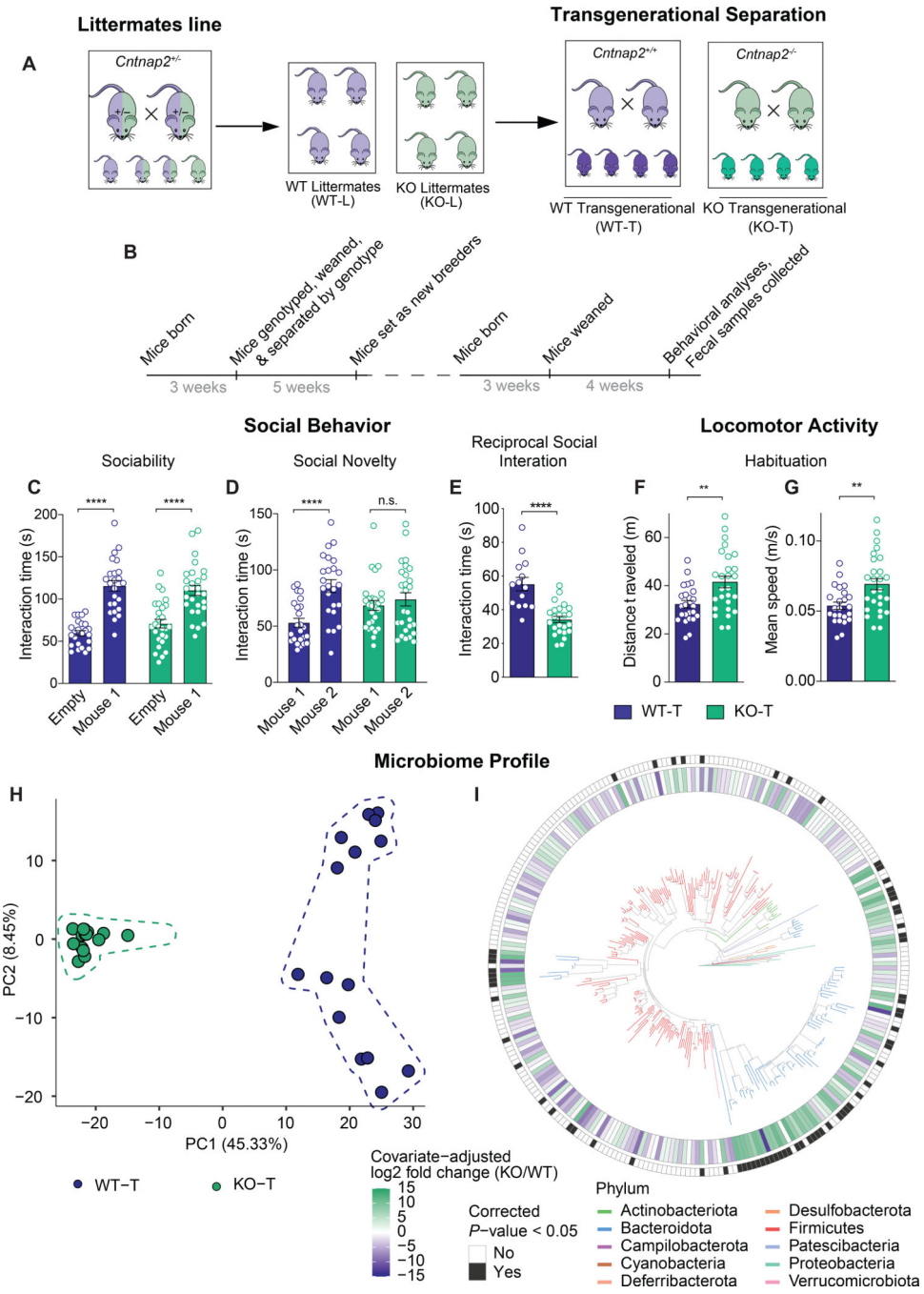

Fig. 4. Transgenerational separation of littermates leads to social deficits and alterations in microbiome composition but does not affect locomotor activity.

A-B, Schemes of the experimental design. **C-D**, Social behavior in WT-T and KO-T mice as assessed in the 3-chamber test (n = 24–27 per group; **C**, Sociability: WT-T: t = 7.182, P < 0.0001; KO-T: t = 5.364, P < 0.0001; two-way ANOVA: $F_{1,98}$ = 0.1254, P = 0.1254; **D**, Social Novelty: WT-T: t = 4.398, P < 0.0001; KO-T: t = 0.7683, P = 0.8883; two-way ANOVA, $F_{1,98}$ = 7.143, P = 0.0088). **E**, Social behavior in WT-T and KO-T mice as assessed in the reciprocal social interaction test, (n = 14–24 per group; WT-T vs KO-T:

Mann-Whitney $U = 30$, $P < 0.0001$). **F-G**, Locomotor activity levels in WT-T and KO-T mice as assessed in the habituation phase of the 3-chamber test ($n = 24–27$ per group; **F**, Distance traveled: WT-T vs KO-T: Mann-Whitney $U = 180$, $P = 0.0060$; **G,** Mean speed: WT-T vs KO-T: Mann-Whitney $U = 180.5$, $P = 0.0061$). **H**, Beta diversity of the 16S rRNA gene sequencing dataset from feces of WT-T and KO-T mice (n = 15 per group) as determined by principal components analysis (PCA) of PhILR-transformed Euclidean (PERMANOVA: $R^2 = 0.44351$, $P = 0.0002$). **I**, Phylogenetic tree of ASVs detected in the 16S rRNA gene sequencing dataset with tree branch colors associated with the phylum of the ASV, the inner circle representing differences in ASV abundance between groups (sliding scale: green = higher in KO, white = no difference, purple = higher in WT), and the outer circle representing the significance level after Benjamini-Hochberg false discovery rate correction (white: not significant, $P \geq 0.05$; black: significant, $P < 0.05$). See also Figure S2, and Table S1, S2.

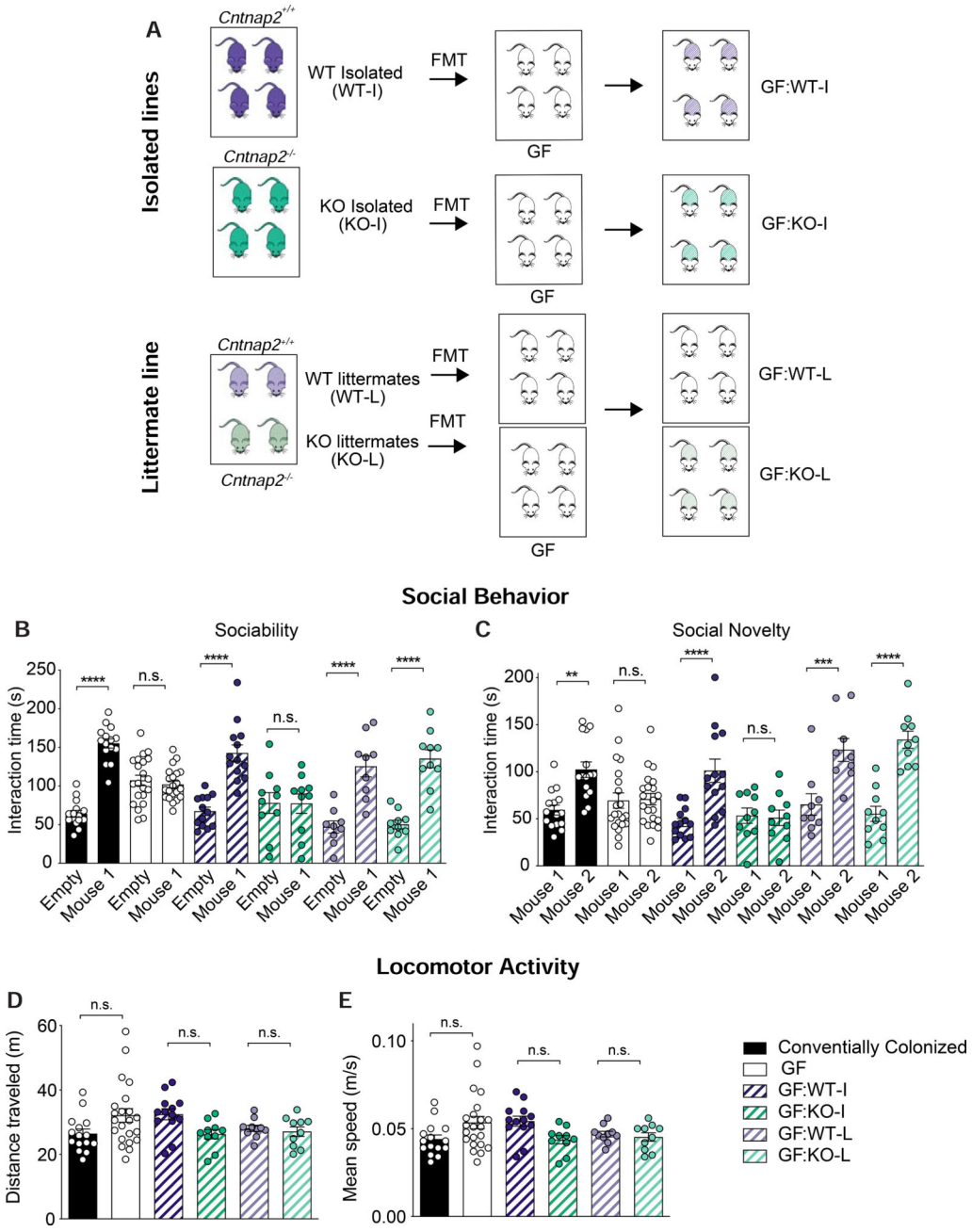

Fig. 5. Microbiota transplantation confers the social behavior phenotype, but not activity phenotype, of the donor lines.

A, Scheme of experimental design for the FMT experiments. **B**-**C**, Social behavior in GF mice transplanted with microbiota from isolated and littermate lines as assessed in the 3-chamber test (n = 9–21 per group; **B**, Sociability: Conventionally Colonized: t = 8.51, P < 0.0001; GF: t = 0.572, P > 0.9999; GF:WT-I FMT: t = 6.557, P < 0.0001; GF:KO-I FMT: t = 0.05714, P > 0.9999; GF:WT-L FMT: t = 5.673, P < 0.0001; GF:KO-L FMT: t = 6.485, P < 0.0001; two-way ANOVA, $F_{5,144}$ = 16.61, P < 0.0001; **C,** Social Novelty: Conventionally Colonized: t = 3.82, P = 0.0012; GF: t = 0.1557, P > 0.9999; GF:WT-I FMT: t = 4.564, P < 0.0001; GF:KO-I FMT: t = 0.1194, P > 0.9999; GF:WT-L FMT: t = 4.006, P = 0.0006;

GF:KO-L FMT: $t = 5.73$, $P < 0.0001$; two-way ANOVA, $F_{5,144} = 7.100$, $P < 0.0001$). **D-E**, Locomotor activity levels in GF mice transplanted with microbiota from isolated and littermate lines as assessed in the habituation phase of the 3-chamber test ($n = 10–22$ per group; **D**, Distance traveled: Conventionally Colonized vs Non-colonized GF: $t = 2.494$, $P = 0.2230$; GF:WT-I vs GF:KO-I: $t = 2.173$, $P = 0.4942$; GF:WT-L vs GF:KO-L: t = 0.3335, $P > 0.9999$; one-way ANOVA: $F_{5,74} = 2.529$, p = 0.0361; **E**, Mean speed: Conventionally Colonized vs Non-colonized GF: $t = 2.501$, $P = 0.2190$; GF:WT-I vs GF:KO-I: $t = 2.218$, $P = 0.4448$; GF:WT-L vs GF:KO-L: $t = 0.3367$, $P > 0.9999$; one-way ANOVA: $F_{5,74} = 2.559$, $P = 0.0343$). See also Figure S3, and Table S1, S2.

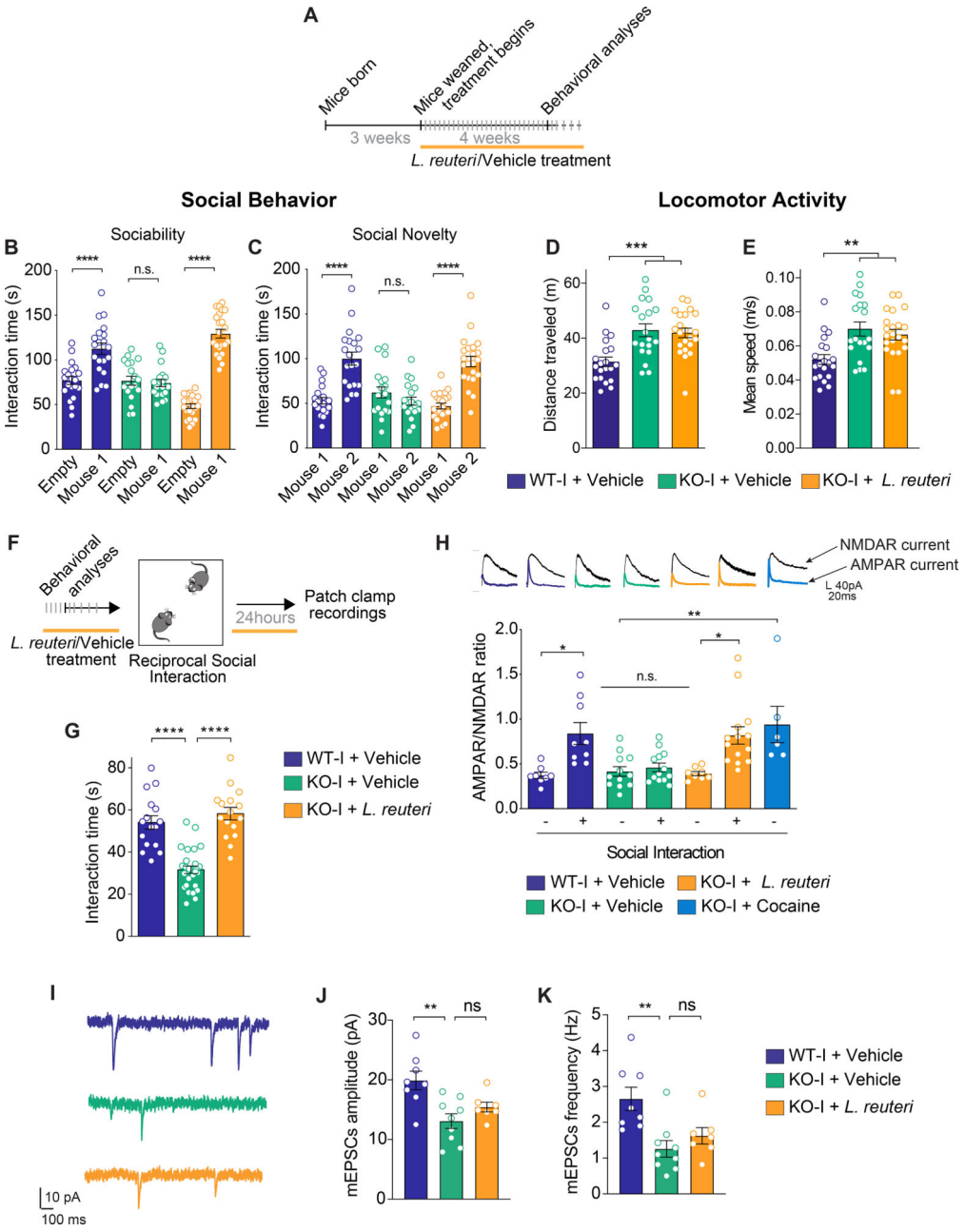

Fig. 6. *L. reuteri* rescues deficits in social behavior and related changes in synaptic transmission without altering locomotor activity levels in *Cntnap2*$^{-/-}$ mice.

A, Scheme of experimental design for the treatment with *L. reuteri*. **B-C**, Social behavior in *L. reuteri* treated mice as assessed in the 3-chamber test (n = 19–22 per group; **B**, Sociability: WT-I + Vehicle: t = 5.329, P < 0.0001; KO-I + Vehicle: t = 0.2167, P > 0.9999; KO-I + *L. reuteri*: t = 12.75, P < 0.0001; two-way ANOVA: $F_{2,116}$ = 36.34, P < 0.0001; **C**, Social Novelty: WT-I + Vehicle: t = 6.228, P < 0.0001; KO-I + Vehicle: t = 1.241, P = 0.6516; KO-I + *L. reuteri*: t = 6.934, P < 0.0001; two-way ANOVA, $F_{2,116}$ = 20.02, P < 0.0001). **D-E**, Locomotor activity levels in *L. reuteri* treated mice as assessed in the habituation phase of the 3-chamber test (n = 19–22 per group; **D**, Distance traveled: WT-I +

Vehicle vs KO-I + Vehicle: $t = 4.143$, $P = 0.0003$; WT-I + Vehicle vs KO-I + *L. reuteri*: $t = 3.935$, $P = 0.0007$; KO-I + Vehicle vs KO-I + *L. reuteri*: $t = 0.3565$, $P > 0.9999$; one-way ANOVA, $F_{2,58} = 10.86$, $P < 0.0001$; **E**, Mean speed: WT + Vehicle vs KO-I + Vehicle: $t = 3.646$, $P = 0.0017$; WT + Vehicle vs KO-I + *L. reuteri*: $t = 3.072$, $P = 0.0097$; KO-I + Vehicle vs KO-I + *L. reuteri*: $t = 0.6995$, $P > 0.9999$; one-way ANOVA, $F_{2,58} = 7.663$, $P = 0.0011$). **F**, Scheme of experimental design for electrophysiological studies. **G**, Social behavior in *L. reuteri* treated mice as assessed in the reciprocal social interaction test (n = 16–28 pairs per group, WT-I + Vehicle vs KO-I + Vehicle: $t = 6.490$, $P < 0.0001$; WT-I + Vehicle vs KO-I + *L. reuteri*: $t = 1.079$, $P = 0.8552$; KO-I + Vehicle vs KO-I + *L. reuteri*: $t = 7.707$, $P < 0.0001$; one-way ANOVA, $F_{2,57} = 37.53$, $P < 0.0001$). **H**, Representative traces of AMPAR and NMDAR currents (top panel) and AMPAR/NMDAR ratio (bottom panel) in VTA DA neurons recorded at baseline and 24 hours after reciprocal social interaction (n = 6–14 per group; WT-I + Vehicle baseline vs WT-I + Vehicle social interaction: $t = 3.462$, $P = 0.0203$; KO-I + Vehicle baseline vs KO-I + Vehicle social interaction: $t = 0.4072$, p > 0.9999; KO-I + Vehicle baseline vs KO-I + *L. reuteri* baseline: $t = 0.1927$, $P > 0.9999$; KO-I + Vehicle baseline vs KO-I + vehicle cocaine: $t = 3.773$, $P = 0.0075$; KO-I + *L. reuteri* baseline vs KO-I + *L. reuteri* social interaction: $t = 3.467$, $P = 0.0201$; one-way ANOVA, $F_{6,63} = 7.119$, $P < 0.0001$). **I**, Representative traces of miniature excitatory post-synaptic currents (mEPSCs). **J**, mEPSCs amplitude (n = 7–9 per group; WT-I + vehicle vs KO-I + vehicle: $t = 3.884$, $P = 0.0026$; KO-I + vehicle vs KO-I + *L. reuteri*: $t = 1.295$, $P = 0.6278$; WT-I + vehicle vs KO-I + *L. reuteri*: $t = 2.385$, $P = 0.0797$; one-way ANOVA: $F_{2,21} = 7.680$, $P = 0.0031$) in WT-I, KO-I and KO-I treated with *L. reuteri.* **K**, mEPSCs frequency (n = 7–9 per group; WT-I + vehicle vs KO-I + vehicle: $t = 3.802$, $P = 0.0031$; KO-I + vehicle vs KO-I + *L. reuteri*: $t = 0.9573$, $P > 0.9999$; WT-I + vehicle vs KO-I + *L. reuteri*: $t = 2.637$, $P = 0.0462$; one-way ANOVA: $F_{2,21} = 7.597$, $P = 0.0033$) in WT-I, KO-I and KO-I treated with *L. reuteri.* See also Figure S4–S5.

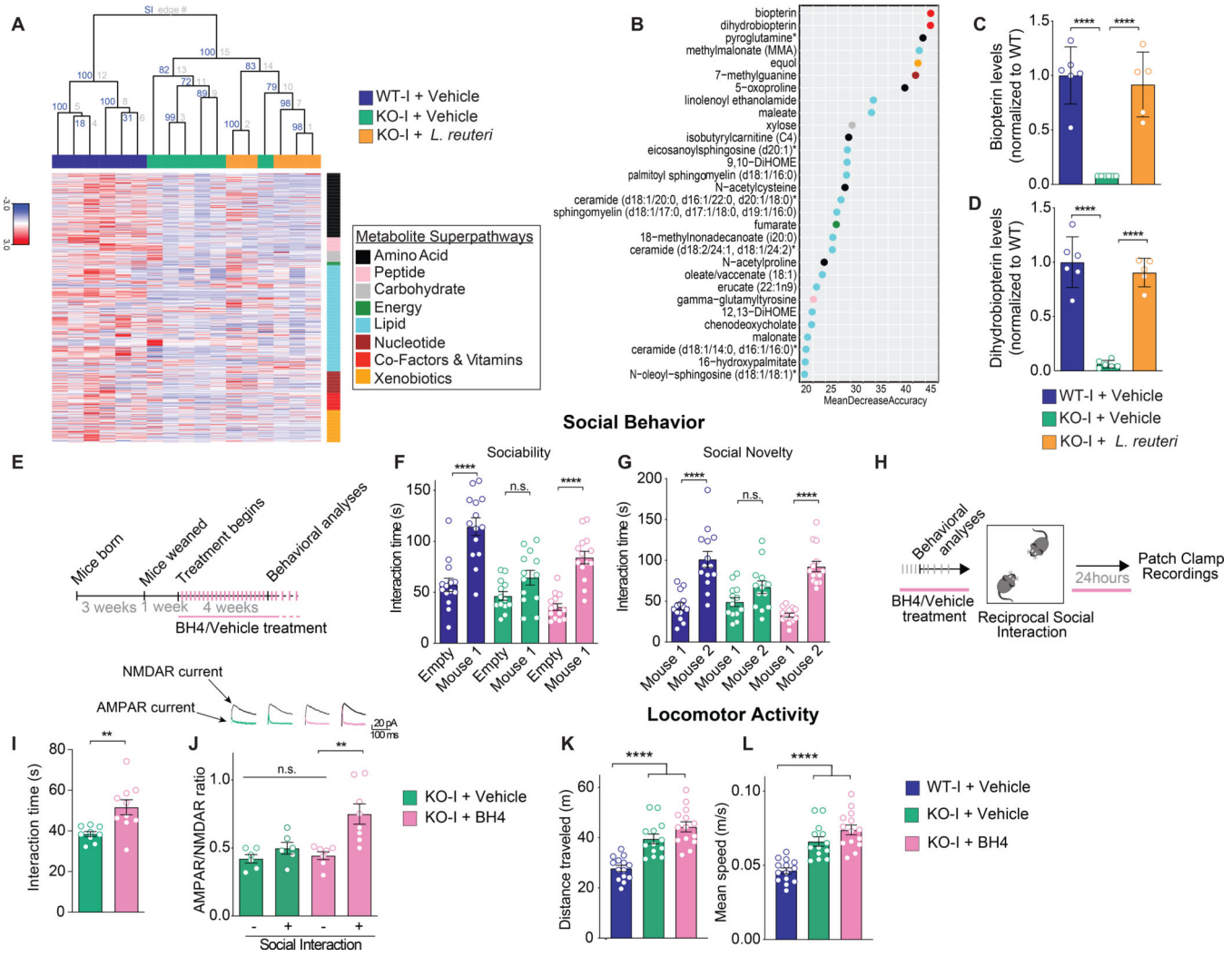

Fig. 7: *L. reuteri* selectively increases metabolites from the tetrahydrobiopterin (BH4) synthesis pathway and BH4 reverses the social deficits (but not locomotor activity levels) in *Cntnap2*$^{-/-}$ mice.

A, Heatmap of hierarchical clustering analysis of fecal metabolites in WT-I + Vehicle, KO-I + Vehicle and KO-I + *L. reuteri*-treated mice (n = 5–6 per group). Selective inference (SI) values (blue) show the stability of each edge (grey) in the tree. **B**, Top 30 most discriminatory fecal metabolites between social (WT-I + Vehicle and KO-I + *L. reuteri*) and non-social (KO-I + Vehicle) groups, identified by Random Forests classification (n = 5–6 per group). **C-D**, Levels of metabolites in BH4 synthesis pathway (n = 5–6 per group; **C**, biopterin: WT-I + Vehicle vs KO-I + Vehicle: t = 7.159, P < 0.0001; WT-I + Vehicle vs KO-I + *L. reuteri*: t = 0.6152, P > 0.9999; KO-I + Vehicle vs KO-I + *L. reuteri*: t = 6.211, P < 0.0001; one-way ANOVA, $F_{2,14}$ = 30.69, P < 0.0001; **D**, dihydrobiopterin: WT-I + Vehicle vs KO-I + Vehicle: t = 10.34, P < 0.0001; WT-I + Vehicle vs KO-I + *L. reuteri*: t = 1.006, P = 0.9944; KO-I + Vehicle vs KO-I + *L. reuteri*: t = 8.852, P < 0.0001; one-way ANOVA, $F_{2,14}$ = 63.40, P < 0.0001). **E**, Scheme of experimental design for BH4 treatment studies. **F-G**, Social behavior in BH4 treated mice as assessed in the 3-chamber test (n = 13–14 per group; **F**, Sociability: WT-I + Vehicle: t = 6.488, P < 0.0001; KO-I + Vehicle: t = 1.968, P

= 0.1581; KO-I + BH4: $t = 5.514$, $P < 0.0001$; two-way ANOA: $F_{2,76} = 5.205$, $P = 0.0076$; **G**, Social Novelty: WT-I + Vehicle: $t = 6.395$, $P < 0.0001$; KO-I + Vehicle: $t = 1.930$, $P = 0.1722$; KO-I + BH4: $t = 6.611$, $P < 0.0001$; two-way ANOA, $F_{2,76} = 6.434$, $P = 0.0026$). **H**, Scheme of experimental design for electrophysiological studies. **I**, Social behavior in BH4 treated mice as assessed in the reciprocal social interaction test ($n = 9$–10 pairs per group, KO-I + Vehicle vs KO-I + BH4: Mann-Whitney $U = 9$, $P = 0.0021$). **J**, Representative traces of AMPAR and NMDAR currents (top panel) and AMPAR/NMDAR ratio (bottom panel) in VTA DA neurons recorded at baseline and 24 hours after reciprocal social interaction ($n = 6$–8 per group; KO-I + Vehicle baseline vs KO-I + Vehicle social interaction: $t = 0.9717$, $P > 0.9999$; KO-I + Vehicle baseline vs KO-I + BH4 baseline: $t = 0.2975$, $P > 0.9999$; KO-I + Vehicle social interaction vs KO-I + BH4 baseline: $t = 0.7109$, $P > 0.9999$; KO-I + BH4 baseline vs KO-I + BH4 social interaction: $t = 4.322$, $P = 0.0015$; one-way ANOVA, $F_{3,23} = 9.125$, $P = 0.0004$). **K-L**, Locomotor activity levels in BH4 treated mice as assessed in the habituation phase of the 3-chamber test ($n = 13$–14 per group; **K**, Distance traveled: WT-I + Vehicle vs KO-I + Vehicle: $t = 4.763$, $P < 0.0001$; WT-I + Vehicle vs KO-I + BH4: $t = 6.833$, $P < 0.0001$; KO-I + Vehicle vs KO-I + BH4: $t = 1.943$, $P = 0.1784$; one-way ANOVA, $F_{2,38} = 24.66$, $P < 0.0001$; **L**, Mean speed: WT + Vehicle vs KO-I + Vehicle: $t = 4.827$, $P < 0.0001$; WT + Vehicle vs KO-I + BH4: $t = 6.853$, $P < 0.0001$; KO-I + Vehicle vs KO-I + BH4: $t = 1.898$, $P = 0.1961$; one-way ANOVA, $F_{2,38} = 24.90$, $P < 0.0001$). See also Figure S6–S7.